AD-A174 280
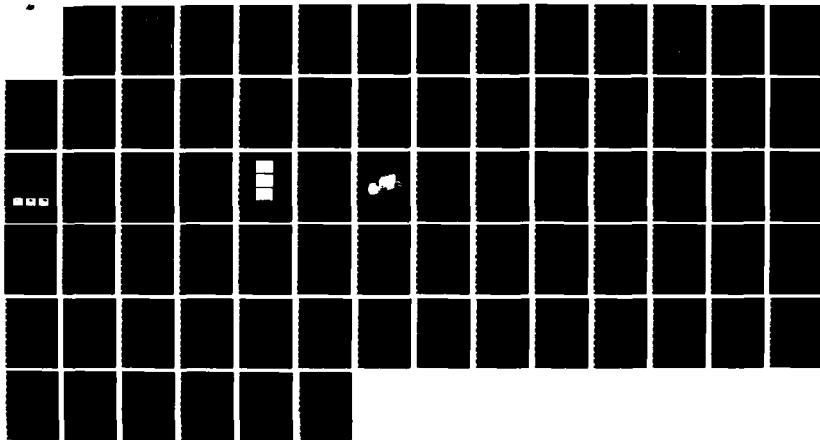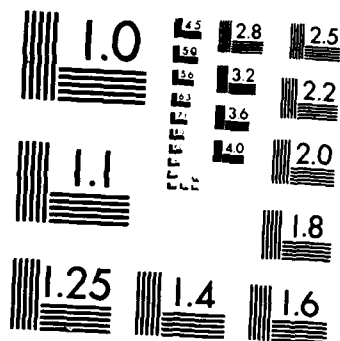
COHERENT LASER SCALING USING OPTICAL PHASE CONJUGATION

G.C. Valley, J.O. White, and R.A. McFarlane

Hughes Research Laboratories

3011 Malibu Canyon Road

Malibu, CA 90265

November 1986

DTIC
SELECTE
NOV 20 1986

A

OFFICE OF NAVAL RESEARCH

800 North Quincy

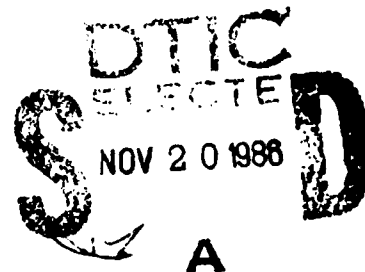Arlington, VA 22217

86 11 20 013

REPORT DOCUMENTATION PAGE

1a. REPORT SECURITY CLASSIFICATION Unclassified		1b. RESTRICTIVE MARKINGS None		
2a. SECURITY CLASSIFICATION AUTHORITY		3. DISTRIBUTION/AVAILABILITY OF REPORT Unlimited		
2b. DECLASSIFICATION/DOWNGRADING SCHEDULE				
4. PERFORMING ORGANIZATION REPORT NUMBER(S)		5. MONITORING ORGANIZATION REPORT NUMBER(S) None		
6a. NAME OF PERFORMING ORGANIZATION Hughes Research Laboratories	6b. OFFICE SYMBOL (If applicable)	7a. NAME OF MONITORING ORGANIZATION Office of Naval Research		
6c. ADDRESS (City, State and ZIP Code) 3011 Malibu Canyon Road Malibu CA 90265		7b. ADDRESS (City, State and ZIP Code) 800 N. Quincy Street Arlington, VA 22217		
8a. NAME OF FUNDING/SPONSORING ORGANIZATION Office of Naval Research	8b. OFFICE SYMBOL (If applicable)	9. PROCUREMENT INSTRUMENT IDENTIFICATION NUMBER ONR/N00014-85-C-0534		
8c. ADDRESS (City, State and ZIP Code) 800 N. Quincy Street Arlington, VA 22217		10. SOURCE OF FUNDING NOS.		
11. TITLE (Include Security Classification) Coherent Laser Scaling Using Optical Phase Conjugation		PROGRAM ELEMENT NO.	PROJECT NO.	TASK NO.	WORK UNIT NO.

10. SOURCE OF FUNDING NOS.			
PROGRAM ELEMENT NO.	PROJECT NO.	TASK NO.	WORK UNIT NO.

12. PERSONAL AUTHOR(S) G.C. Valley, J.O. White, R.A. McFarlane			
13a. TYPE OF REPORT Interim Report	13b. TIME COVERED FROM Aug 85 TO Aug 86	14. DATE OF REPORT (Yr., Mo., Day) November 1986	15. PAGE COUNT 75

16. SUPPLEMENTARY NOTATION

17.	COSATI CODES		18. SUBJECT TERMS (Continue on reverse if necessary and identify by block number)
FIELD	GROUP	SUB. GR.	Phase Conjugation, Beam combining, Nonlinear optics

19. ABSTRACT (Continue on reverse if necessary and identify by block number)

Coherent combining of pulsed dye gain media through phase conjugation in photorefractive barium titanate is reported. Phase and frequency locking of two and three pulsed dye lasers is demonstrated for both narrowband cavities (0.05 nm) and broadband cavities (0.25 nm). Oscillator configurations are used throughout in order to avoid geometries that require a master oscillator or a master laser and slave laser.

20. DISTRIBUTION/AVAILABILITY OF ABSTRACT UNCLASSIFIED/UNLIMITED ☒ SAME AS RPT ☐ OTIC USERS ☐	21. ABSTRACT SECURITY CLASSIFICATION Unclassified	
22a. NAME OF RESPONSIBLE INDIVIDUAL G. C. Valley	22b. TELEPHONE NUMBER (Include Area Code) (213) 317-5435	22c. OFFICE SYMBOL

DD FORM 1473, 83 APR   EDITION OF 1 JAN 73 IS OBSOLETE.

TABLE OF CONTENTS

Accession For

NTIS GRA&I

DTIC TAB

Unannounced

Justification

By

Distribution/

Availability Codes

Avail and/or

Dist   Special

A-1

LIST OF ILLUSTRATIONS

SECTION 1

INTRODUCTION

This report presents interim results for the first year of a
three year program on coherent laser scaling using optical phase
conjugation. The purpose of this program is to demonstrate that
multiple laser oscillators can be coherently and efficiently
coupled through nonlinear optical phase conjugation processes.
The work includes invention of effective coupling geometries,
investigation of alternative conjugators, and evaluation of all
system parameters that affect laser coupling. These parameters
include conjugator properties such as linewidth, reflection
coefficient, fidelity, angular field of view, and intensity
dependence. In addition, gain medium properties – such as the
small-signal gain coefficient, the saturation intensity, the
linewidth, and the spatial extent – affect the coupling process.
Finally, we are investigating the use of auxiliary elements to
assist the coupling process. These elements include apertures,
lenses, line-narrowing prisms, etalons and gratings, and
attenuators.

Initial studies during the first phase of this program have
been directed towards understanding the coupling of pulsed dye
oscillators with self-pumped conjugators in photorefractive
$BaTiO_3$. We chose to investigate this system for a number of
reasons. First, the combination of oscillators with self-pumped
conjugation in $BaTiO_3$ could potentially lead to a very simple
system--possibly as simple as one crystal, n dye cells and n
outcoupling mirrors. Second, the use of pulsed, high-peak-power,
broadband oscillators provides a test system from which results
may be extrapolated for a number of important applications. The
dye cells are expected to provide a good prototype for coupling
high-power excimer gain media or Nd:YAG rods. Third, dye cells
are compact and inexpensive so multiple modules can be added
without major perturbations to the program schedule or budget.

7

Fourth, self-pumped conjugators in $BaTiO_3$ are easy to make, and can be made in at least six independent geometries. Thus, they can be used to simulate a wide range of conjugation processes, including those that may be more difficult to work with, or those that may be more readily scalable to high powers. Finally, to our knowledge, coupling of an all-oscillator system has not been demonstrated; yet it provides an excellent system to which modules can be added, because all modules are equivalent. This flexibility contrasts, for example, with the master/slave coupling experiments or the master-oscillator, power amplifier experiments performed previously.

We have obtained a number of interesting coupling results in the first year of this program. We have demonstrated phase- and frequency-locking of two dye oscillators in several configurations. We have demonstrated coupling of three oscillators. We have also investigated a number of pseudo-coupling systems in which two or three oscillators were only partially coupled.

Section 2 contains a review of the self-pumped conjugators discovered to date. Previous combining results are reviewed in Section 3. Following description of our interim results in Section 4, Section 5 gives a brief summary of future work planned in this program.

SECTION 2

SELF-PUMPED CONJUGATORS

Real-time phase conjugation dates from the investigations of stimulated Brillouin scattering (SBS) by Zel'dovich et al.[1] in 1972, and it is now possible to produce phase conjugate beams at wavelengths from the near ultraviolet to the far infrared (see the review by Pepper[2]). Although a wide range of processes have been used to produce conjugate beams, limiting consideration to self-pumped conjugators with no external pump beams narrows the list to SBS and self-pumped photorefractive materials. In the original proposal for this program,[3] we decided to limit consideration to beam-combining with self-pumped conjugators for two reasons — simplicity and efficiency. The major alternative, four-wave mixing, has added complexity because it requires two additional pump beams of good beam quality, and is probably less efficient because of the power needed for the pumps.

Stimulated Brillouin scattering conjugators have many attractive features. They are relatively compact, requiring gas or liquid cells less than a meter long. They are efficient, producing reflectivities up to 90%, and they can produce excellent conjugation fidelity under many conditions.[4] Complicated optics are not required, and SBS conjugators' fields of view are relatively large. SBS is, however, a threshold process, and obtaining good reflectivities and conjugation fidelities requires operation at power levels substantially above threshold. For 10-ns pulses, as in our system, the typical threshold energy is about 1 mJ for a single pulse of an unaberrated beam, so efficient conjugation of a beam with some spatial structure would require perhaps 10 mJ. This energy level is more than can be comfortably obtained with our pump laser and multiple dye cells, so our initial studies have concentrated on the self-pumped photorefractive conjugators. The self-pumping

9

process in photorefractive materials also has an energy threshold, but these materials have storage capability so multiple pulses can be used to surpass the threshold, whereas in SBS threshold must be reached within one pulse.

At least six independent self-pumped conjugators have been demonstrated in photorefractive materials. Since they all may prove useful for beam combining, and since one of them may prove to be optimal, we will discuss them in detail. Figure 2-1 shows the first self-pumped photorefractive conjugator, discovered by White et al.[5] In this conjugator, beam fanning starts oscillation between two mirrors that form a Fabry-Perot-like cavity. The counterpropagating beams in this cavity become phase conjugates of each other as the beam fanning coalesces into a single channel, and finally a phase conjugate beam is returned through four-wave mixing.

The second self-pumped conjugator, shown schematically in Figure 2-2, was discovered by Feinberg.[6] In this device, beam fanning diffracts incident radiation into the corner of a crystal where it is retro-reflected into the fanning interaction region. For reasons that are not completely understood, this fanning also coalesces into two or more thin channels of light and leads to the reflection of a high-quality phase conjugate beam. Because this conjugator lacks external mirrors, it is less sensitive to vibrations and seems to produce better fidelity than the one shown in Figure 2-1. On the other hand, the threshold gain-length product required for this conjugator is somewhat larger than that for the Fabry-Perot conjugator.

The third conjugator has external mirrors arranged in a ring cavity around the crystal of $BaTiO_3$,[7] as shown in Figure 2-3. This device generates only one of its pump beams by stimulated photorefractive scattering, is self-starting, and has a lower threshold than the second conjugator. This conjugator is also insensitive to external mirror vibrations.
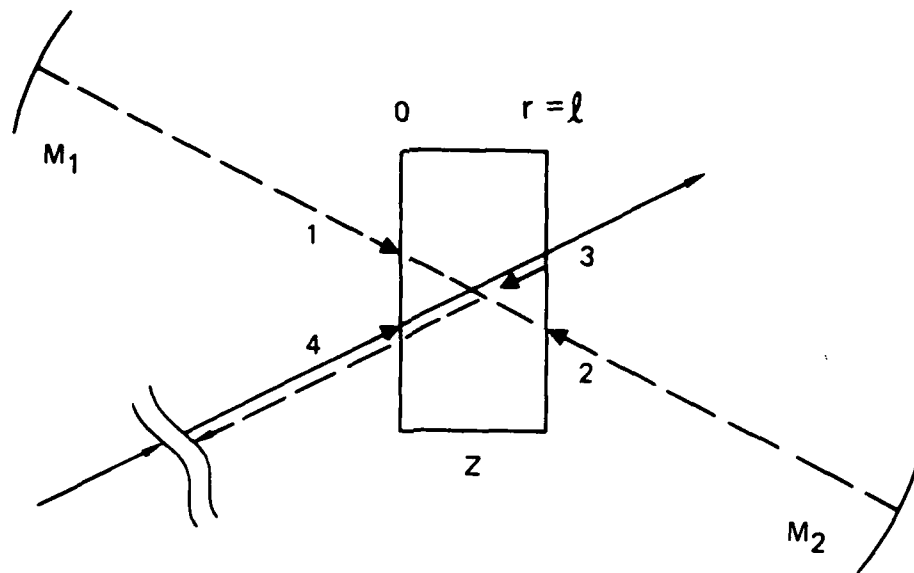
Figure 2-1. Self-pumped conjugator in $BaTiO_3$ using a Fabry-Perot resonator.[5] The upper mirror may be blocked or removed after self-pumping begins.
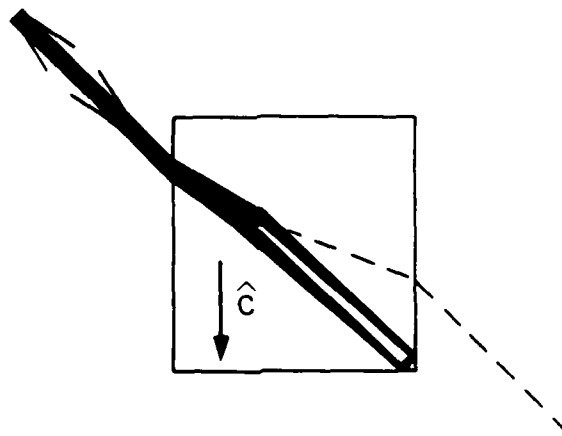
Figure 2-2. The internally self-pumped conjugator using a corner reflection and beam fanning in $BaTiO_3$.[6]
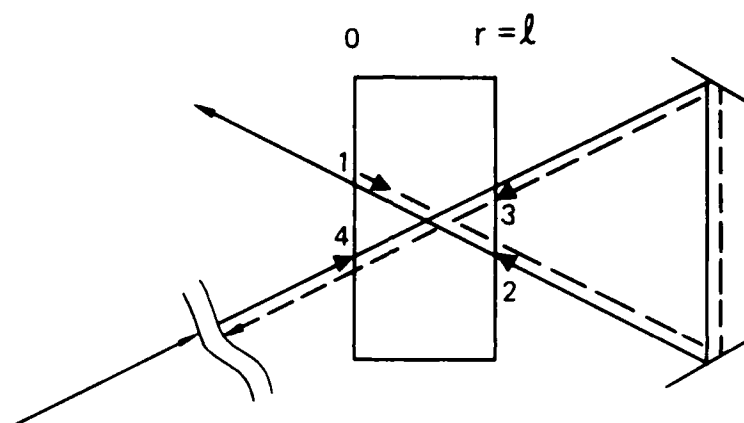
Figure 2-3.   The ring self-pumped conjugator geometry.[7]

In 1985 Günter introduced a new variation on the internal self-pumped conjugator by painting the surface of his crystal with "white office correcting paint, Tipp-Ex."[8] As shown in Figure 2-4, this geometry does not require fanning into the corner of the crystal. The large volume of reflected light may be especially useful for combining lasers.

Also in 1985, Chang and Hellwarth[9] found that stimulated photorefractive backscattering could be used to produce a phase conjugate wave in a manner analogous to stimulated Brillouin scattering. Their interaction geometry is shown in Figure 2-5. Gain-length requirements are significantly higher than for the others, but this conjugator may be useful for beam coupling if it allows a larger field of view.

Recently, the self-pumped double-phase conjugate mirror has been demonstrated by Sternklar et al.[10] As shown in Figure 2-6, this self-pumped conjugator provides two phase conjugate outputs for two incoherent input beams. The conjugate beams in this device are spatial conjugates, but, unlike the other conjugators, are temporally incoherent with the input beams. Initial studies of laser interaction using this conjugator have been reported by Sternklar et al.[10]

In our initial studies of beam combining with self-pumped $BaTiO_3$ conjugators, we decided to use the internally self-pumped conjugator discovered by Feinberg and shown in Figure 2-2. We made this choice because the conjugator is simple to construct, we had already used it with pulsed dye lasers to make a phase conjugate resonator (PCR),[11] and it was known to have a wide field of view.[12] Figure 2-7 shows measurements of the reflectivity as a function of external angle to the crystal obtained from Ref. 12. Note that in the region from 32° to 89° the reflectivity exceeds 1, which gives rise to self-oscillation. In order to obtain maximum likelihood of lasing, we have aligned our resonators to intersect the initial self-pumping beam in this angular region.
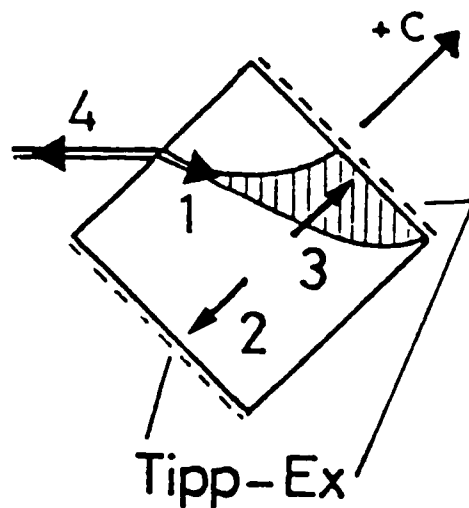
Figure 2-4.   The internally self-pumped
              conjugator using internal
              reflection from Tipp-Ex paint.[8]
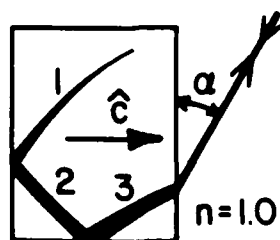
Figure 2-5.   The stimulated photo-
              refractive backscattering
              conjugator that operates
              analogously to the SBS
              conjugator.[9]
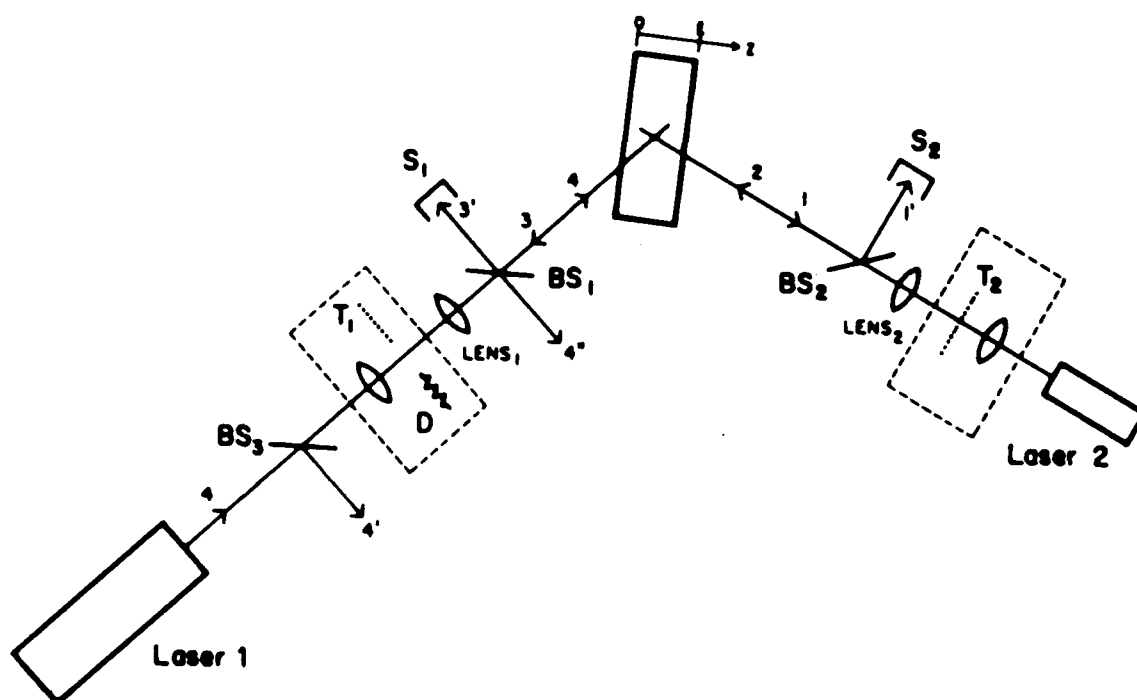
Figure 2-6. The double-phase conjugator mirror
that conjugates two incoherent
input beams.[10]
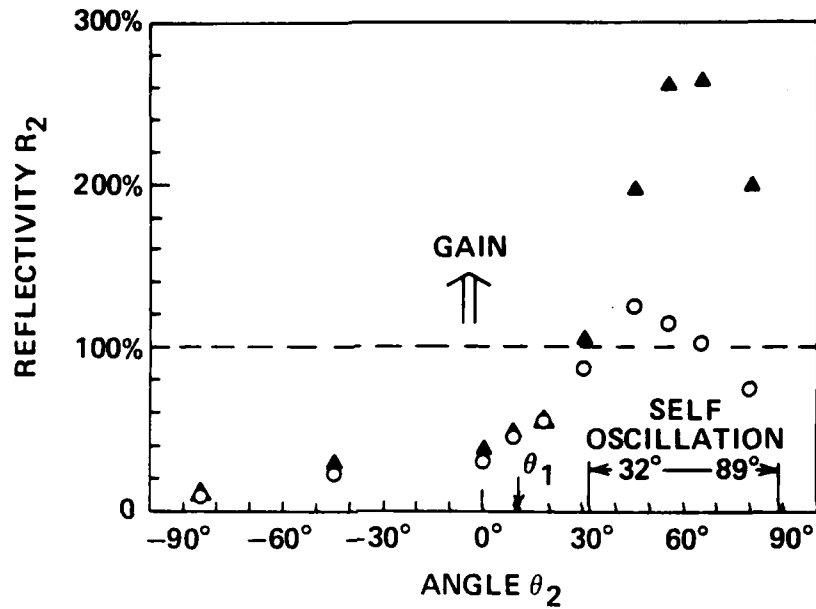
Figure 2-7. Reflectivity as a function of angle around the main beam in an internally self-pumped conjugator.[12]

SECTION 3

BEAM COMBINING THROUGH NONLINEAR PHASE CONJUGATION

Results on combining multiple lasers or beams through a
common nonlinear phase conjugate mirror have recently been
published by many groups.[13-19] This work has used both
stimulated Brillouin scattering conjugators[13,14,19] and the
photorefractive conjugators discussed in Section 2.[15-18] In the
early work of Basov,[13] shown in Figure 3-1, a combination of SBS
and hypersonic four-wave mixing was used in a master-oscillator
power-amplifier (MOPA) configuration to couple nine independent
regions of a 1.06-μm-wavelength gain medium. While details of
the experiment and the results are vague in Ref. 13, it is clear
that introduction of a common phase conjugate mirror for all nine
beams produced substantial improvement in beam quality. No
explicit results on phase- or frequency-locking are presented.
The complexity of this system is clear from Figure 3-1. The
system requires a master oscillator and an auxiliary beam for the
SBS processes. Coherence requirements for these beams are
unstated, while relative power levels are vaguely discussed. For
scaling to high powers, neither the master oscillator nor the
auxiliary beam is desirable.

More recently, Rockwell and Giuliano[14] have demonstrated
locking of two Nd:YAG gain media with the double-pass MOPA system
shown in Figure 3-2. In this work a conventional SBS phase
conjugate mirror with a common interaction region was used, and
far-field patterns of the two beams were presented to demonstrate
phase locking. In related work, workers at TRW showed that two
beams are locked when combined in a common interaction region in
an SBS conjugator, but that the locking disappears when the
overlap of the beams is reduced.[19] We have observed the
analogous process in some of our attempts to lock oscillators in
photorefractive $BaTiO_3$.

AUXILIARY
BEAM

MASTER
OSCILLATOR

1/4λ

NINE
CHANNEL
1.06 μm AMPLIFIER

SBS
(HYPERSONIC)
CELL
2

SBS
1
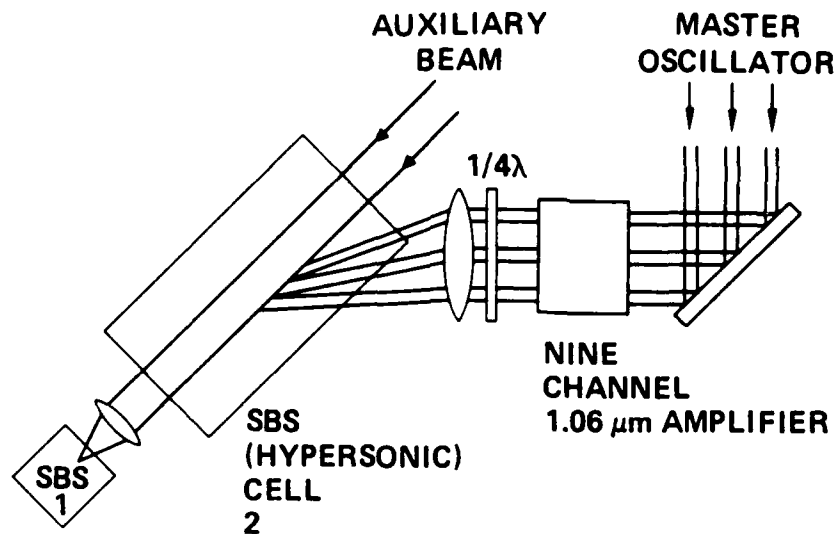
Figure 3-1. Beam combining using a master-oscillator
power-amplifier configuration, nine gain
regions in a 1.06-μm-wavelength amplifier,
and hypersonic four-wave mixing.[13]

16244-6

Nd:YAG
OSCILLATOR

BEAM
EXPANSION
TELESCOPE

2X CYLINDRICAL
TELESCOPE

λ/4

THIN FILM
POLARIZER

Nd:YAG
AMPLIFIERS

TILTED
APERTURES

MIRROR

SBS PHASE
CONJUGATE
MIRROR
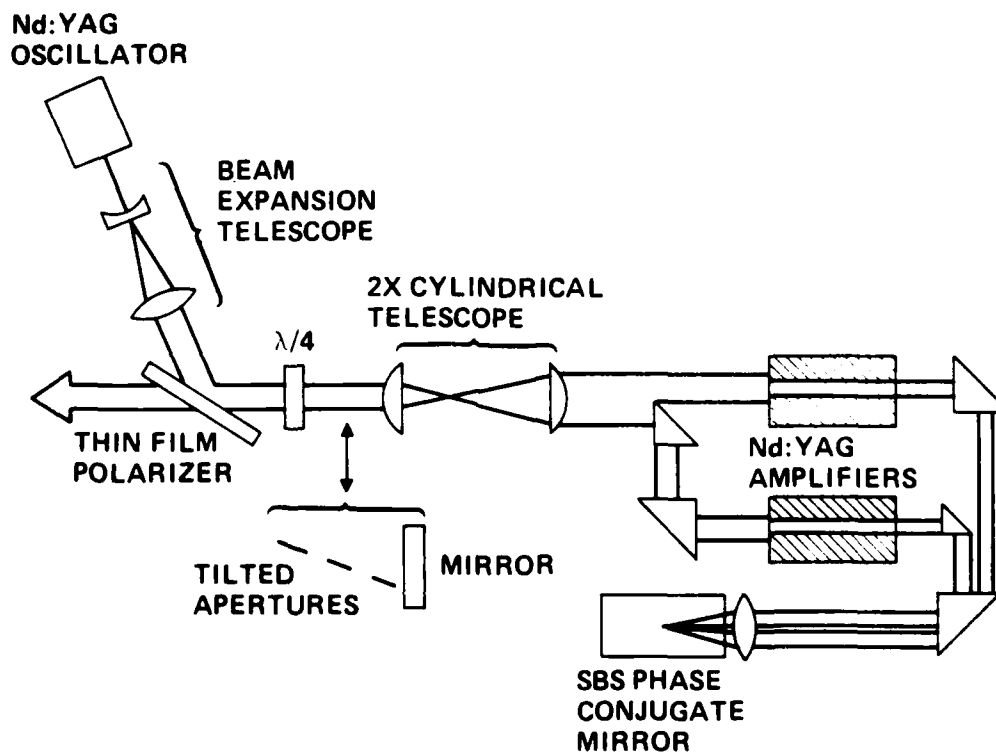
Figure 3-2. Combining two Nd:YAG amplifiers with a
double pass MOPA configuration and an
SBS conjugator.[14]

18

The first results of using self-pumped conjugation in $BaTiO_3$ to lock lasers were publish- ' by Feinberg and Bacher.[15] As shown in Figure 3-3, they used the internally self-pumped conjugator geometry of Figure 2-2 to lock two argon-ion lasers. The first laser made the self-pumped conjugator and functioned as a master laser; its end mirrors were never removed. The second laser was an argon-ion laser with one of its end mirrors removed. Results showed that energy from the master laser cavity was coupled through the four-wave mixing process in $BaTiO_3$ into the slave cavity. No frequency spectra or interference patterns of the two beams were presented to prove locking, although the results are not inconsistent with the behavior of frequency locked lasers. Results on self-scanning in $BaTiO_3$ conjugators[24] and the double-phase conjugate mirror,[10] in which incoherent beams appear to write a grating with each other, indicate that the lasers might be coupled in some way without frequency- or phase- locking. The slave cavity might start from the master but jump away in frequency as the slave power is turned up. Without spectra or interference patterns this possibility is difficult to rule out. No results or configurations without the master laser were presented in Ref. 15. For scaling to high powers or large numbers of modules, master-laser configurations may be a disadvantage, since the master laser power may provide a fundamental limitation on performance. Understanding or removing this limitation has been one of the goals of this program, as discussed in Section 4.

Phase locking of two independent self-pumped $BaTiO_3$ conjugators has been demonstrated by Ewbank et al.[18] Their results show that a locking beam can grow from noise to connect the relative phase of two self-pumped conjugators. This technique may be useful for laser scaling, as it allows multiple conjugators to be linked.

$BaTiO_3$ is also sensitive in the infrared,[22,23] which suggested its use to couple diode lasers.[16,20] In Ref. 16, the ring self-pumped geometry of Figure 2-3 was used to couple master and slave GaAlAs diode lasers as shown in Figure 3-4. While both lasers had high reflection coatings on the rear facet and

19
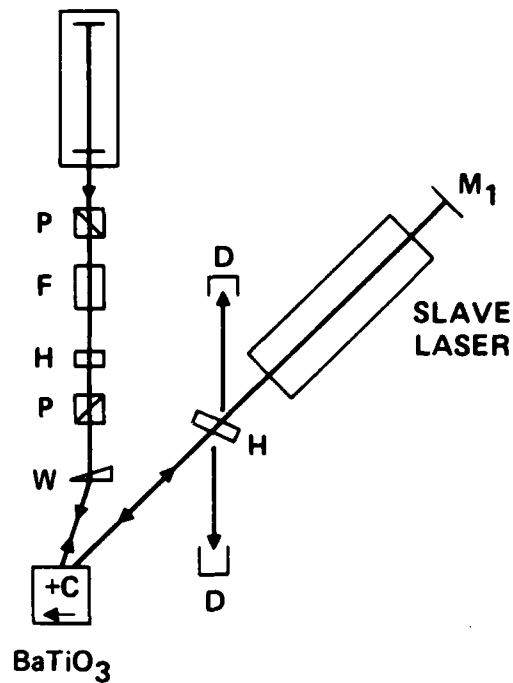
MASTER
LASER

P = LINEAR POLARIZER, F = FARADAY CELL,
H = HALF-WAVE PLATE, W = WEDGED FLAT,
D = DETECTOR, M₁ = MIRROR

Figure 3-3. Combining a master argon-ion laser
and a slave laser through internally
self-pumped conjugation in $BaTiO_3$.[15]
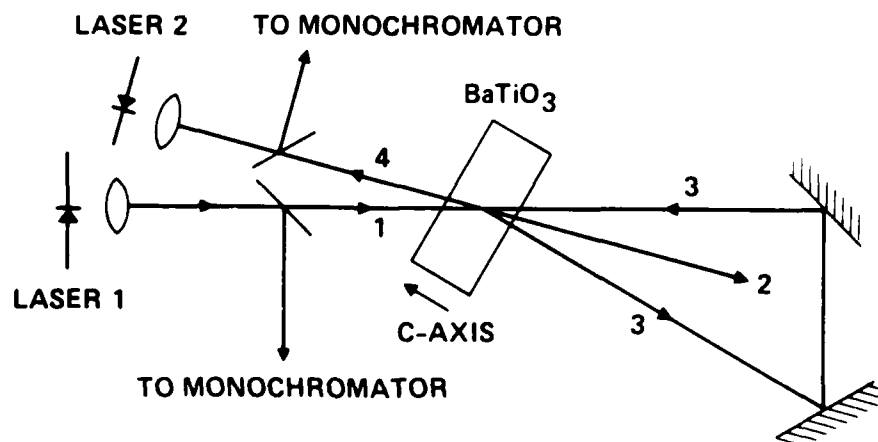
Figure 3-4. Combining two diode lasers through
the ring self-pumped conjugator.[16]

antireflection coatings on the front facet, they were capable of lasing without the phase conjugator. Thus, as with the work of Feinberg and Bacher, this work uses a master/slave configuration. Frequency spectra presented in Ref. 16 showed that the two diodes start with multiple longitudinal mode operation, and that then their frequency spectra collapse to a single overlapping longitudinal mode. When the feedback between the lasers is removed, the frequency of one laser moves away from that of the two together: this appears to be unequivocal evidence of frequency locking.

Recently, Hughes Research Laboratories (HRL) has demonstrated coupling of a single multistrip gain medium through a MOPA configuration using a self-pumped $BaTiO_3$ conjugator as shown in Figure 3-5.[20] Our results show coupling of the entire gain medium through the use of a conjugator. In other work in progress at HRL, we are performing beam locking in a four-wave mixing geometry in sodium, as shown in Figure 3-6.[21] This work does not rely on a shifted grating conjugator or on a self-pumped conjugator; it is intended to couple oscillators and to be scalable to high powers.

12637-112
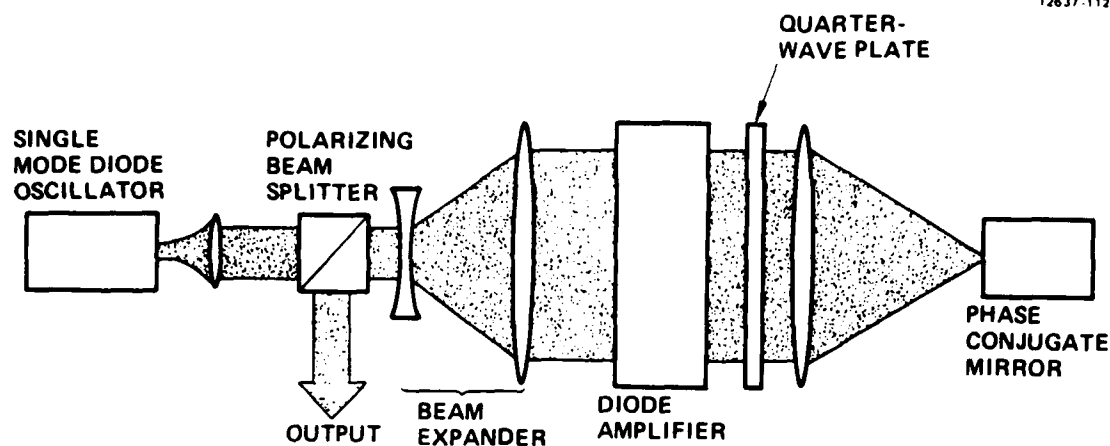
FEATURES

- SINGLE FREQUENCY
- EXCELLENT BEAM QUALITY   } HIGH BRIGHTNESS
- HIGH POWER

Figure 3-5.   Coupling a multistrip diode amplifier through
a MOPA configuration and a ring self-pumped
conjugator.[20]

16244-1
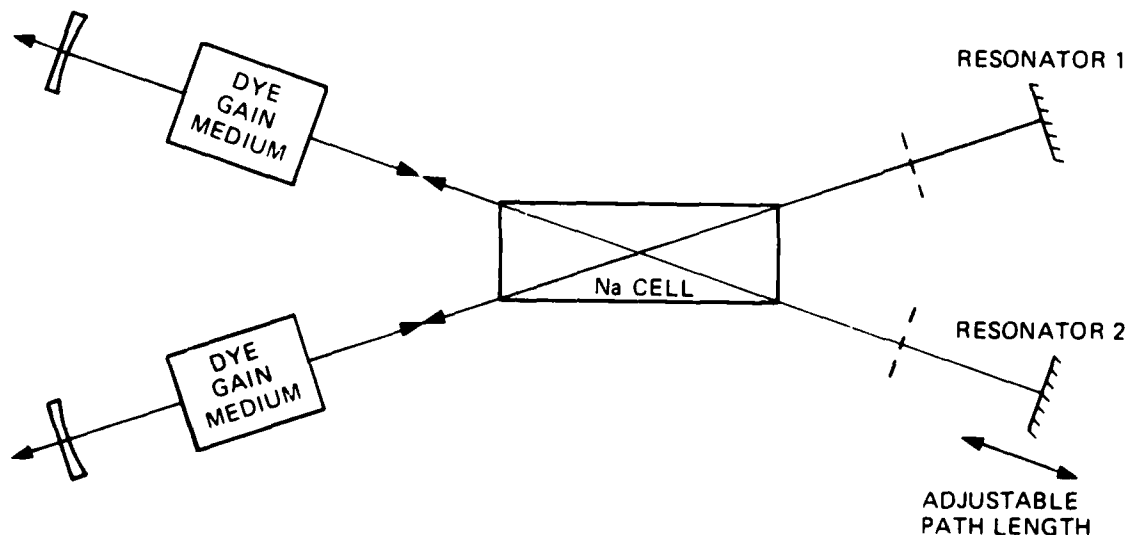
Figure 3-6.   Concept for coupling through four-wave
mixing in a sodium cell.[21]

22

SECTION 4

BEAM COMBINING RESULTS

A. COMBINING TWO PULSED DYE MODULES

Our beam combining studies began with two Nd:YAG-pumped dye
cells in the geometry shown in Figure 4-1. The doubled Nd:YAG
pump is a commercial (Quantel) laser operating at a wavelength of
0.532 μm with a repetition rate from 1 to 10 Hz, a pulse length
of approximately 10 ns, and an energy-per-pulse up to several
hundred millijoule. This device was typically operated far below
its maximum output, as less than a millijoule is typically needed
to pump a single dye cell. In the first experiments, the beam
expander and grating in cavity 1 were replaced by a second prism
assembly. Unlike past experiments with a 1-kHz string of 100-ns
pulses, self-pumped conjugation proved to be difficult to obtain
for 10-Hz, 10-ns pump pulses using the dye cavity narrowed with
the three-prism tuner. When one of the prism assemblies was
replaced by the beam-expander, grating combination, self-pumped
conjugation was easily achieved. One result was obtained with
the system with two prism assemblies, however. In this result
both cavities were observed to lase as PCRs, using the BaTiO$_3$ as
one end mirror and the prisms and conventional mirrors as the
other end mirror. Close inspection of the beam patterns in the
crystal suggested that two separate self-pumping processes were
occurring simultaneously. Furthermore, blocking laser 1 had no
effect on laser 2's output, and vice versa. We concluded that
the cavities were not locked in this experiment.

In the geometry shown in Figure 4-1, the BaTiO$_3$ is immersed
in oil of refractive index 1.5. This immerson has two beneficial
effects. First, it allows beams to enter the BaTiO$_3$ in such a
way as to access larger angles to the crystal c axis inside the
crystal. This typically gives higher coupling coefficients (see
Ref. 24, reprinted in Appendix A). Second, the oil allows a
larger angular extent in which to bring the second beam. The
wide field of view experiments performed by Feinberg were
performed with the crystal immersed in oil for this reason.[13]

23
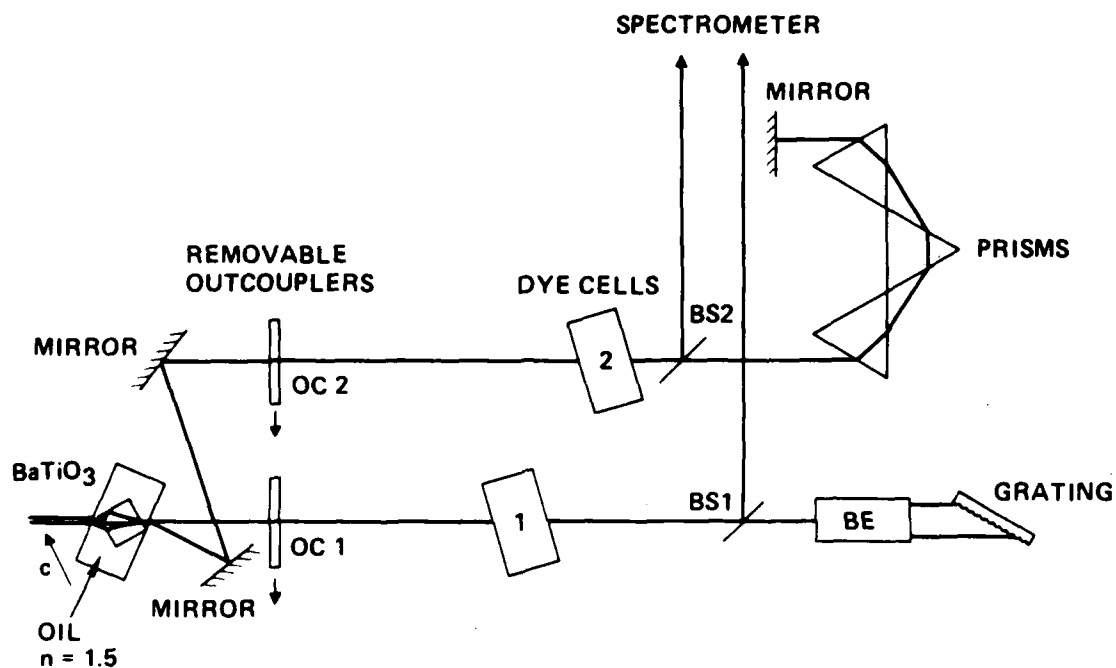
Figure 4-1. Optical schematic for the system used
to couple two narrowband dye oscillators.
BS = beamsplitter, BE = beam expander,
OC = outcoupler.

24

The spectrometer shown in Figure 4-1 is a commercial unit (Candela LS-1) with a resolution of 0.01 nm that can be improved to 0.001 nm with the addition of an optional etalon. In addition to spectral width measurements, the spectrometer can provide absolute wavelength information, although this feature was rarely used. The dye cells are filled with a mixture of rhodamine 6G and methanol, with the concentration set to absorb approximately 90% of the pump light. The cells are glass cuvettes obtained from NSG Precision Cells, and are glued to magnetic stirrers from Tri-R Instruments. Outcouplers 1 and 2 are partially reflecting mirrors on swivel mounts. The beam expander is a commercial unit (Spectra-Physics) and the grating (SA Instruments) operated in the Littrow configuration has 1800 lines per mm. The 0.532-μm beams propagate into the dye cells at a slight angle to the axis of the dye laser cavity. Typically, the diameter of the green pump beams is 1 to 2 mm at the cells.

Coupling of the two cavities was reliably obtained by the following procedures. First, lasing was obtained between OC1 and the grating with the $BaTiO_3$ blocked and the green pump to dye cell 2 blocked. Then the crystal was unblocked, and within approximately one minute self-pumped conjugation, as shown in Figure 2-2, was obtained. (At this point OC1 can be removed, resulting in a PCR analogous to that discussed in Ref. 11.) Then the upper turning mirror from cavity 2 was blocked and cavity 2 was allowed to lase by unblocking the pump to dye cell 2. Cavity 2 was tuned so that its broadband output spectrally overlapped the narrowband output of cavity 1. At this point the upper mirror was unblocked and radiation from cavity 2 propagated towards the crystal. After approximately 30 to 60 seconds OC2 could be removed and cavity 2 slowly grew in power with a narrow linewidth. Figure 4-2(a) shows the spectrum of cavity 2 lasing off outcoupler 2 with no radiation from the laser falling on the crystal (broad spectrum), and later lasing with OC2 removed and the crystal coupling cavities 1 and 2 (narrow spectrum). Note that the narrowband master oscillator did not have to be tuned to the center of the broadband laser for the system to work. The narrow line is nearly identical to the spectrum of cavity 1 alone, shown in Figure 4-2(b).
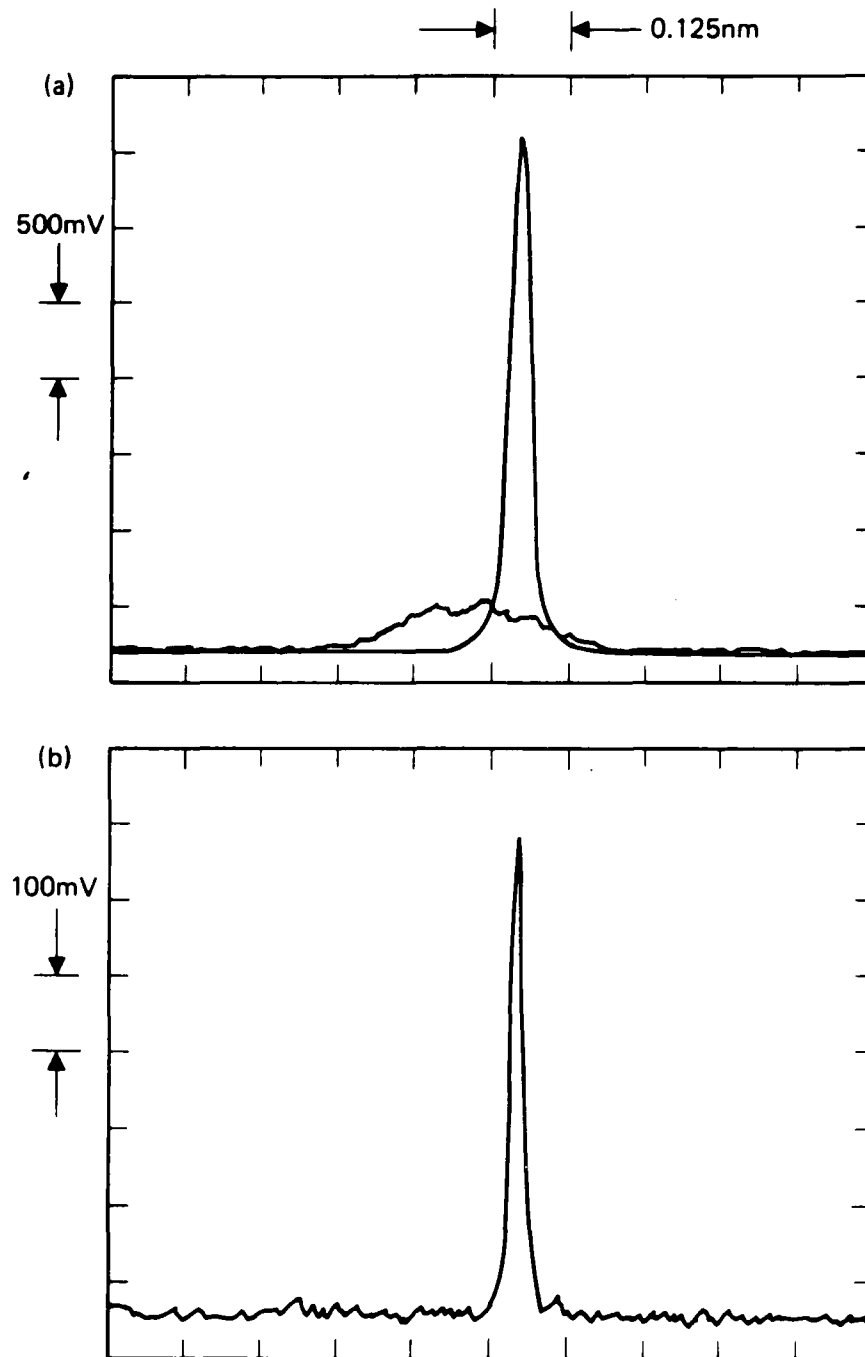
Figure 4-2. Spectra of cavities 1 and 2.
(a) Cavity 2, operating broadband with
OC2 and operating narrowband without
OC2 and locked to cavity 1. (b) Cavity 1
operating with OC1 and grating.

Figure 4-3(a) shows the spectra of cavities 1 and 2 when they are coupled. Within the resolution of the spectrometer the two lasers have the same wavelength and nearly identical linewidth. When cavity 1 is blocked, cavity 2 no longer has access to a fixed line narrowing element (the grating), and its radiation relaxes to the broader spectrum shown in Figure 4-3(b). Without a frequency reference, this cavity then spontaneously self-scans, as has been observed before in self-pumped PCRs using photorefractive $BaTiO_3$ and dye lasers.[24] Beams from the two cavities with the spectra as shown in Figure 4-3(a) were arranged to interfere with each other and produced the fringe pattern shown in Figure 4-4(c). With the results shown in Figure 4-3(a) and 4-4(c), we have demonstrated frequency locking and spatial phase locking of narrowband pulsed dye lasers. We observed, in addition, that if we blocked one cavity, the power out of the other cavity dropped, and vice versa. Note that the final system consists of two coupled oscillators. In contrast to the experiments of Feinberg and Bacher[15] and those of Cronin-Golomb et al.,[16] this device does not contain a master laser that will continue to lase in the absence of phase conjugate reflection. The only remnant of the master/slave concept in this system is the existence of the beam expander and grating in cavity 1.

B. COMBINING THREE DYE OSCILLATORS

Our investigation of the coupling of three dye cells used the system shown in Figure 4-5. It was found that the line-narrowing prisms were not necessary to couple cavities if the end mirrors were properly aligned with respect to the pump direction and the radiation from the other cavities at the $BaTiO_3$. We have been able to operate the system shown in Figure 4-5 both narrowband (approximately 0.05 nm linewidth) and broadband (0.25 nm). The devices and the starting procedures are slightly different in each case.
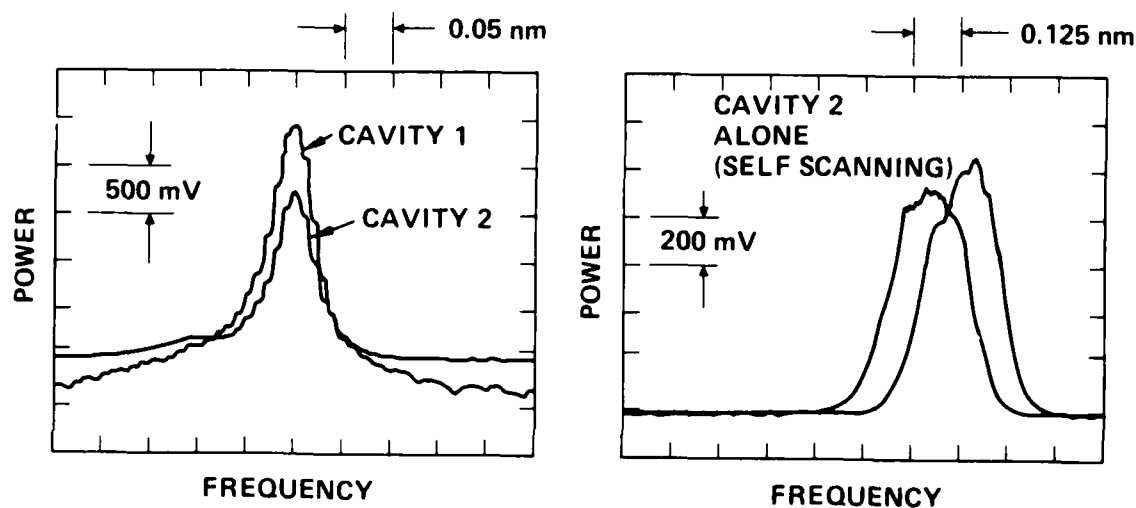
Figure 4-3. (a) Spectra of two locked cavities. (b) Cavity 2 operating as a broadband PCR with cavity 1 blocked. The two spectra were taken approximately 1 min apart and illustrate the self-scanning of dye PCRs operated with self-pumped $BaTiO_3$ mirrors.

4-4(a)   4-4(b)   4-4(c)
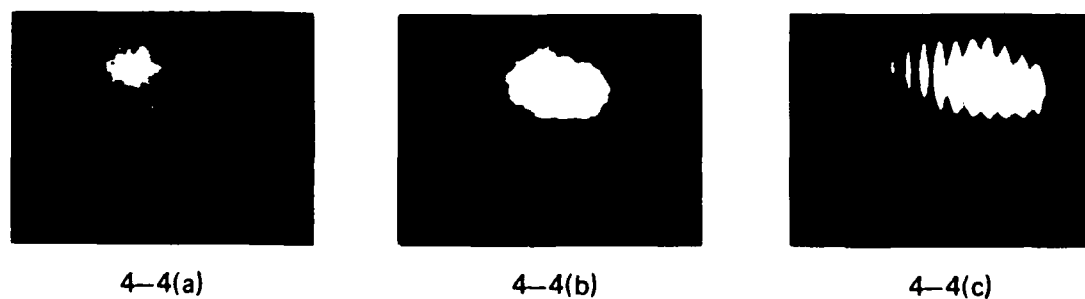
Figure 4-4. Interference fringes of two coupled dye oscillators. (a) Beam from cavity 1 alone, (b) Beam from cavity 2 alone, (c) Interference pattern.

28
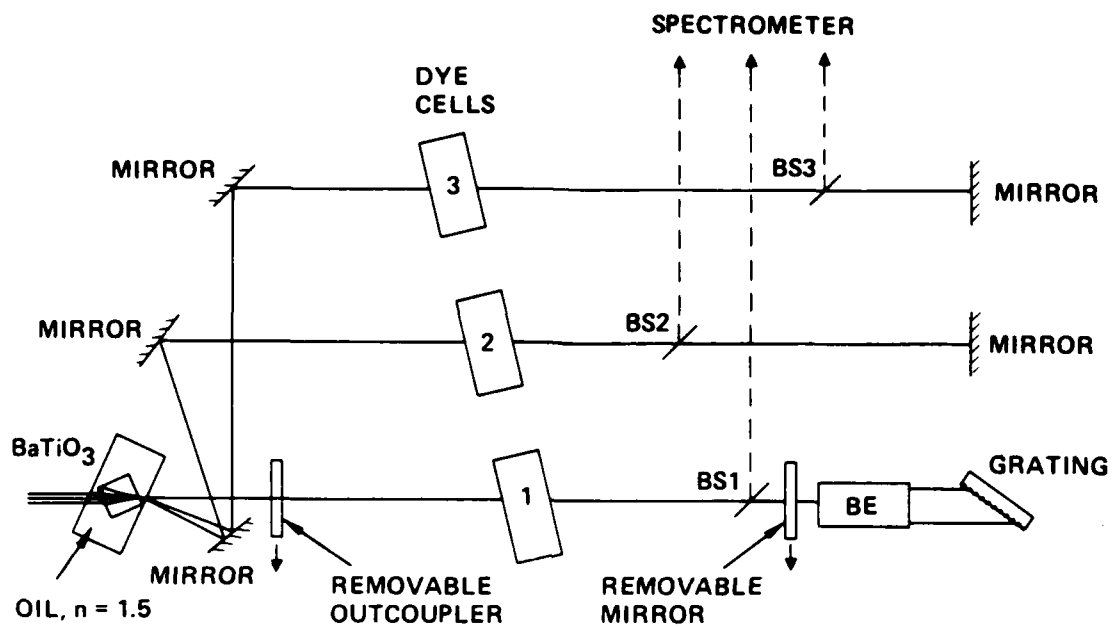
Figure 4-5. Optical schematic of three dye cell system.

For the narrowband device, the starting procedures are
essentially as described above. The only adjustments required
are steering the super-radiance into the crystal by tilting the
right end mirrors of cavities 2 and 3 instead of tuning the
prisms. Spectra for the narrowband operation, as shown in Figure
4-6, are essentially the same as those for two cavities as shown
in Figure 4-3(a). Further tests of the power coupling and phase
locking of this device are in progress.

A three-cavity system consisting only of three end mirrors,
three dye cells, and one crystal has also been operated using the
components shown in Figure 4-5. This system is obtained by
starting cavity 1 narrowband as described above, but when it is
operating as a PCR (i.e., with the left outcoupling mirror
removed), a high reflectivity mirror is inserted between the beam
expander and the dye cell. The spectral width of cavity 1 slowly
broadens to about the width shown by Figure 4-3(b) (cavity 1 is
now essentially the same device as that whose spectrum is shown
in Figure 4-3(b)). Cavity 1 may self-scan, and it is helpful to
wait for this to stabilize. Then cavities 2 and 3 can be started
from their own super-radiance, giving the spectra shown in
Figure 4-7. These procedures have not been consistently
repeatable at present, and other anomalous behavior has been
observed. For instance, we have observed one or more of the
cavities spectrally break away from the rest and self-scan to
different operating points — that is, the lasers spontaneously
unlock. Alternatively, when turning on the third cavity, we have
observed that it can extinguish one or both of the other
cavities. A reproducible and consistent start-up procedure is
being sought.
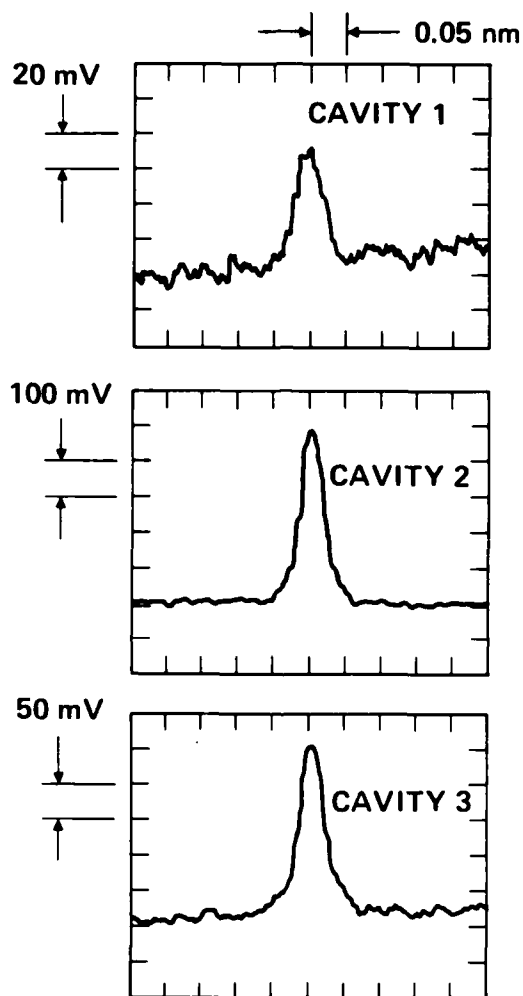
Figure 4-6. Spectra of three coupled dye
oscillators in which cavity 1
has the beam expander and grating
for a line narrowing element.
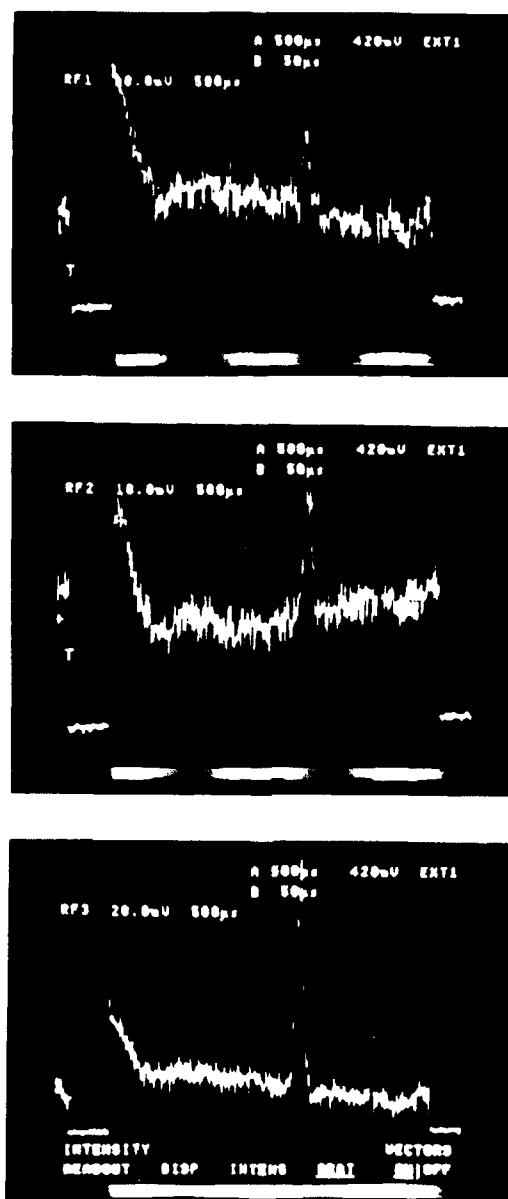
Figure 4-7. Spectra of three coupled dye oscillators with no line narrowing element in any cavity (1 div. = 1.25 nm).

SECTION 5

FUTURE WORK

The phase- and frequency-locking experiments with three
cavities are approximately half completed. A better
understanding of how to make this system operate efficiently is
required. Comparison of the scales of Figures 4-6 and 4-7 with
those of Figure 4-3(a) shows that the power levels in the three
cavity system are substantially lower. It should be emphasized
that these are only qualitative relationships because no attempt
has been made at present to measure the absolute pump power
delivered to the dye cells. In addition, it will be useful to
make interference patterns for the three beam system.

Absolute measurements of power output of one, two, and three
dye cell systems are also important. Little is gained in
coupling three lasers if this results in less power output than
one alone could provide. Thus absolute measurements may require
further investigation of the reflectivity of the self-pumped
conjugator or the use of other conjugator geometries.

A third area of near term work is illustrated in Figure 5-1,
which shows a four dye-cell module. Use of this module is
expected to result in a more compact system and perhaps more
efficient operation. This system will also be used to perform
efficiency measurements.

A more detailed discussion of future work under this program
has been given in Ref. 25.

33
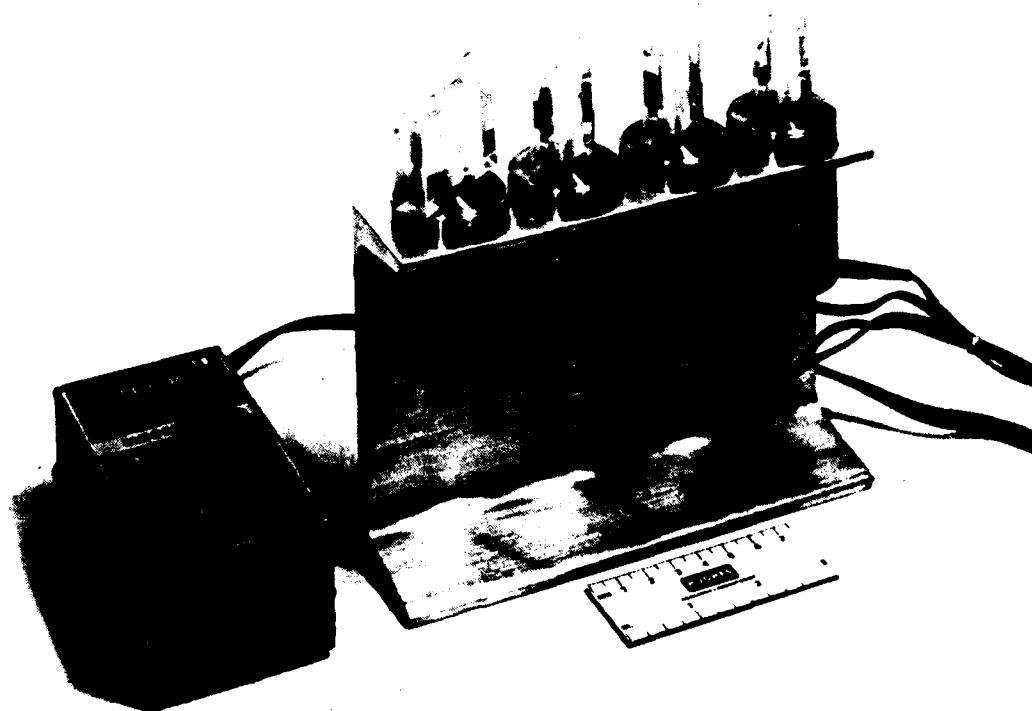
Figure 5-1.   Picture of a four dye cell module for future work.

REFERENCES

1. B. Ya. Zel'dovich et al., Sov. Phys. JETP Lett. **15**, 109 (1972).

2. D.M. Pepper, Ch. 4 in **Laser Handbook Vol.4**, ed. M.L. Stitch and M. Bass (Amsterdam: North-Holland, 1985).

3. Coherent Laser Scaling Using Optical Phase Conjugation, Hughes Research Laboratories Proposal 85M-0451/F9282 (April 1985).

4. B. Ya. Zel'dovich et al., **Principles of Phase Conjugation**, (New York: Springer-Verlag, 1985).

5. J.O. White et al., Appl. Phys. Lett. **40**, 450 (1982).

6. J. Feinberg, Opt. Lett. **7**, 486 (1982).

7. M. Cronin-Golomb et al., Appl. Phys. Lett. **41**, 689 (1982).

8. P. Günter et al., Opt. Commun. **55**, 210 (1985).

9. T.Y. Chang and R.W. Hellwarth, Opt. Lett. **10**, 408 (1985).

10. S. Sternklar et al., Opt. Lett. **11**, xxx (1986).

11. R.A. McFarlane and D.G. Steel, Opt. Lett. **8**, 208 (1983).

12. J. Feinberg, Opt. Lett. **8**, 569 (1983).

13. N.G. Basov et al., Sov. J. Quantum Electronics **11**, 1335 (1981).

14. D.A. Rockwell and C.R. Giuliano, Opt. Lett. **11**, 147 (1986).

15. J. Feinberg and G.D. Bacher, Appl. Phys. Lett. **48**, 570 (1986).

16. M. Cronin-Golomb et al., Appl. Phys. Lett. **48**, 1240 (1986).

17. S. Sternklar et al., Opt. Lett. **11**, 528 (1986).

18. M.D. Ewbank et al., Opt. Lett. **10**, 282 (1985).

19. M. Valley et al., J. Opt. Soc. Am. B **3**, xxx (1986)

20. Blue Laser Transmitter Technology, Hughes Aircraft Company Technical Proposal 84M-0562/F6873, (May 1984).

21. Coupled Resonators Modeling Techniques, Hughes Aircraft Company Technical Proposal 84M-0818/F7417 (June 1984).

22. M. Cronin-Golomb et al., **47**, 567 (1985).

23. B.T. Anderson et al., **10**, 627 (1985).

24. W.B. Whitten and J.M. Ramsey, Opt. Lett. **9**, 44 (1984).

25. Coherent Laser Scaling Using Optical Phase Conjugation, Phases II and III, Part 2--Technical Proposal 86M-0568/F9282-2 (June 1986).

Appendix 1

Competition between forward and backward
stimulated photorefractive scattering in BaTiO$_3$

George C. Valley

Hughes Research Laboratories

3011 Malibu Canyon Road

Malibu, CA 90265

Abstract

The gain length product for two-wave mixing in photorefractive BaTiO$_3$ is calculated as a function of the angles between a pump beam and a scattered beam and the crystal c axis. The gain-length product at times shortly after turning on the pump often shows a maximum for backscattering while the steady-state gain-length product is usually maximized for near forward scattering (an angle of about 10° between the pump and scattered beams). The calculations suggest that backscattering will be optimized in a hole-dominated crystal with a large trap density.

37

1. INTRODUCTION

Stimulated photorefractive scattering (SPS) may be defined as the selective amplification via the photorefractive effect of optical radiation scattered by medium inhomogeneities. In $BaTiO_3$, a single pump beam incident on the crystal may produce stimulated scattering in the near forward direction (beam fanning)[1], in the backward direction[2], in a ring surrounding the pump beam[3,4], and in a variety of other complicated patterns[5,6]. The dominance of one process over another depends on a number of factors such as the angle between the pump beam and the crystal c axis, the polarization of the pump beam, the angle between the amplified noise and the pump, crystal geometry, crystal imperfections, and aberrations on the pump beam. As is the case for stimulated Raman or Brillouin scattering, SPS is either the desired result in a device (e.g. production of a conjugate wavefront[2]) or a source of noise that reduces the performance of a device. The purpose of this paper is to use the theory of the photorefractive effect developed by Kukhtarev[7] and current knowledge of the properties of $BaTiO_3$ to understand the angular dependence of SPS for a single pump beam in the plane of the crystal c axis. In particular, it is desirable to understand how backscattering can dominate forward scattering in $BaTiO_3$ even though

38

steady-state gain calculations suggest that the gain in the backward direction (grating period equal to $0.1 \mu m$) should always be substantially less than that in the forward direction (grating periods of a few microns).[8] SPS out of the plane of the pump and c axis[3,4] is not discussed in this paper.

Many terms have been used previously to describe SPS: photoinduced light scattering,[9-11] anisotropic light scattering,[3,12] asymmetric light scattering,[9] asymmetric self-defocusing,[1] beam fanning,[1] degenerate stimulated parametric scattering,[13] and photoinduced Rayleigh scattering.[8,14,15] The term optical damage has been used to refer to the refractive index gratings left behind by SPS. SPS has a rich history and in fact the first well-defined observation of the photorefractive effect involves SPS in $LiNbO_3$ and $LiTaO_3$.[16] Since then SPS has been investigated further in $LiNbO_3$[3,4,11,12,17-19], $LiTaO_3$[3,13], $(Sr_xBa_{1-x})_{1-y}(Nb_2O_6)_y$[9,10], and $BaTiO_3$.[1-6,14]

Detailed predictions of the intensity and direction of SPS in $BaTiO_3$ are complicated by features of the interaction that depend on the specific crystal (size, cut, surface roughness, and optical quality). These properties and the angular spectrum of the pump control the strength of the noise waves that are selectively amplified by the two-wave mixing process. In fact, some of the "noise" waves may actually be Fresnel reflections of the pump beam from the

39

crystal-external medium interface or from crystal striations. Despite these difficulties, an assessment of the relative "chances" of noise waves at various angles to the pump beam can be obtained by calculating two quantities as a function of the angle between the noise wave and pump and the angle to the c axis: (1) the gain length product at short times and (2) the steady-state gain coefficient. The first quantity is related to the noise start-up while the second is related to which beams dominate at long times. Unfortunately, neither quantity predicts the start-up or the steady-state exactly. This is because selective amplification cannot start until the two-wave mixing gain for an individual noise beam exceeds its loss. Thus one needs to solve the time dependent wave equations until gain equals loss to determine which beams can grow in a real crystal. Then in order to determine which beam dominates in the steady state the calculations must proceed into the pump depletion regime. Such solutions of the nonlinear wave equations in time and in two or three dimensions would be very interesting but besides being beyond the scope of this work, would be specific to a single crystal and depend for instance on the details of the material inhomogeneities, Fresnel reflections, etc. that start SPS in a particular geometry.

2. BASIC EQUATIONS

The calculations proceed from the set of equations given by Kukhtarev et al.[20] for two optical amplitudes A_p and A_s (pump and scattered waves) and the space charge field E:

$$\partial A_p / \partial x_p = -i(1/2)(k/n_p)r_{eff}A_s E \tag{1}$$

$$\partial A_s / \partial x_s = -i(1/2)(k/n_s)r_{eff}A_p E^* \tag{2}$$

$$\partial E/\partial t + E/\tau = iE_{sc}A_p A_s^* / [\tau(|A_p|^2 + |A_s|^2)] \tag{3}$$

where x_p and x_s are coordinates along the directions of propagation of the pump and scattered waves, n_p and n_s are the refractive indices in those directions, $k = 2\pi/\lambda$ (λ is the vacuum wavelength and any detuning or frequency shift between the pump and scattered waves is ignored)), r_{eff} is the effective electro-optic coefficient, and τ is the space charge field and refractive index grating decay rate. E_{sc} and τ are given by

$$E_{sc} = E_0 / (1 - E_0/E_q) \tag{4}$$

$$\tau = \tau_{di}(1 - E_0/E_w)/(1 - E_0/E_q) \tag{5}$$

and $E_0 = k_B T k_g/e$, $E_q = eN_A(1-N_A/N_D)/(\epsilon\epsilon_o k_g)$, $E_w = 1/(k_g\mu\tau_R)$ and $\tau_{di} = \epsilon\epsilon_o/(e\mu n_c)$. Also, $k_B T$ is Boltzmann's constant times temperature, k_g is the grating wavenumber, e is the magnitude of the charge on an electron, ϵ_o is the permittivity of free space, ϵ is the dielectric constant, μ is the mobility, n_c is the mean carrier number density which equals $\alpha(|A_p|^2 + |A_s|^2)\tau_R/h\nu$ ($h\nu$ is the energy per photon),

41

and the remaining symbols are defined in the Table. These equations are applicable to crystals of $BaTiO_3$ in which one charge carrier dominates. In crystals in which both electrons and holes participate[21], a more complicated theory is required.[22,23]

For extraordinary polarization r_{eff} is given by[24]

$$r_{eff} = \{n_o^4 r_{13}\cos\theta_p\cos\theta_s + 2n_e^2 n_o^2 r_{42}\cos^2[(\theta_p+\theta_s)/2]$$
$$- n_e^4 r_{33}\sin\theta_p\sin\theta_s\} \sin[(\theta_p+\theta_s)/2] \qquad (6)$$

where θ_p and θ_s are the angles between the pump and scattered waves and the c axis as shown in Fig. 1. In $BaTiO_3$ both the mobility and the dielectric constant are known to be anisotropic:[25,26]

$$\mu = \mu_{11}\sin^2\theta_c + \mu_{33}\cos^2\theta_c \qquad (7)$$

$$\epsilon = \epsilon_{11}\sin^2\theta_c + \epsilon_{33}\cos^2\theta_c \qquad (8)$$

where θ_c is the angle between the grating normal and the c axis.

In the calculations that follow, the effective interaction length l_{eff} has been modeled with the formula:

$$l_{eff} = L(1 - \exp[-d/(L \sin 2\theta)]) \qquad (9)$$

where L is the length of the crystal in the direction bisecting the two beams, d is the diameter of the beams and θ is half of the angle between the beams $[\theta = (\theta_s - \theta_p)/2]$. This model for l_{eff} reduces to L for parallel and antiparallel beams $[d/(L\sin 2\theta) \gg 1]$ to d for beams crossing at right angles [i.e. for $d/(L\sin 2\theta) \ll 1$, $l_{eff} = d/\sin 2\theta$]. A more detailed calculation would depend on

specifics of the crystal/beam geometry, but this model includes the most important effect; namely, beams crossing with angles near 90° have a much smaller effective interaction length than those propagating nearly parallel or antiparallel.

The steady-state, small-signal, gain-length product for amplification of noise waves, G_{ss}, is obtained by dropping the $\partial E/\partial t$ term in eq. (3) and substituting eq. (3) into eq. (2). For amplification of noise waves, $|A_s|^2$ is small compared to $|A_p|^2$ until pump depletion becomes important and G_{ss} is given by

$$G_{ss} = (1/2)(k/n_s)r_{eff}E_{sc}l_{eff} \tag{9}$$

The gain length product per absorbed energy per volume at turn-on is obtained by neglecting the second term on the left hand side of eq. (3), integrating eq. (3), substituting the result into eq. (2) and factoring out the quantity $\alpha(|A_p|^2 - |A_s|^2)t$, which is the absorbed energy per unit volume (the units of the quantities $|A_s|^2$ and $|A_p|^2$ are assumed to be W/cm^2). Then G_{to} is given by

$$G_{to} = (1/2)(k/n_s)r_{eff} \ e \ \mu\tau_R E_0 \ l_{eff}/[\epsilon\epsilon_o \ (1 + E_0/E_M)]. \tag{10}$$

43

3. RESULTS

Results for the steady-state gain length product G_{ss}
and the product per absorbed energy per volume at turn-on
G_{to} are shown in Figs. 2 and 3 for the baseline parameters
given in the Table and the geometry shown in Fig. 1. The
optical wavelength is taken to be $\lambda = 0.5\mu m$, the beam
diameter $d = 1mm$, and the crystal width $L = 5mm$. As a
baseline the trap density is $N_A = 10^{17}$ cm^{-3}. In these
figures the angle between the pump and the c axis varies
from 0° to 90° and the scattered beam angle varies from the
pump angle to the c axis to that angle plus 360°. These
figures are for a crystal in which the charge carriers are
holes. Figures for electron-dominated crystals are obtained
by changing the sign of the ordinate as are results for a
crystal in which the c axis points in the opposite
direction. Flipping the crystal c axis by 180° is
equivalent to changing the pump angle into the 180 to 270°
quadrant so Figs. 2 and 3 can be used immediately for the
pump beams in the first and third quadrant about the c axis.
The figures for the 90 to 180° quadrant are obtained by
turning Figs. 2 and 3 upside down. Results similar to
parts of Fig. 3 for the near forward, steady-state gain[34]
and for the steady state backscatter gain[15,32] have been
given previously (The result in Ref. 15 differs from that

given here and in Ref. 32 because the anisotropy in the
dielectric constant ϵ was neglected in Ref. 15).

The steady-state gains in Fig. 3 are in agreement with
the observations and estimates of Chang and Hellwarth.[2] In
particular, for angles of the pump beam to the c axis of 20°
to 40° the backscatter gain is G_{ss} = 10. Allowing a factor
of 2 for phase conjugationin in the backward direction[35]
yields $G_{ss,conj}$ = 20, which compares favorably with the
gains usually required for phase conjugation via stimulated
Brillouin scattering.

The results in Fig. 2 suggest the answer to the
question of how backscattering can dominate near forward
scattering. While the steady-state gain is larger for near
forward scattering, the gain at turn-on is larger in the
backward direction for most angles of the pump to the c
axis. The physical reason for this is that charge carriers
can diffuse the small grating period formed by the
counterpropagating beams much more efficiently than the
large period grating of the near forward scattering. This
same effect can be seen in previous calculations of the
photorefractive sensitivity (refractive index change per
absorbed energy per unit volume) [Fig. 8 of Ref. 8]. If the
mobilities are increased by a factor of ten, the dominance
of the backward gain at turn-on disappears as seen in Fig. 4
for a pump angle to the c axis of 30°. Note that G_{to} in the
backward direction (θ_s = 210°) is nearly the same in Fig. 4

45

as in Fig. 3 (for $\theta_p = 30°$) while G_{t_0} is substantially increased in the near forward direction.

Fig. 5 illustrates how the results shown in Figs. 2 and 3 change if the trap density is reduced by a factor of 5 to $N_A = 2 \times 10^{16}$ cm^{-3} for pump angle to the c axis $\theta_p = 30°$. In Fig. 5a the increase in gain at turn-on is due to the increase in the recombination time for the smaller trap density of $N_{A.} = 2 \times 10^{16}$ cm^{-3}. This increase in recombination time gives the carriers a larger diffusion length and makes the material more sensitive, especially in the near forward direction where the grating period is large. In Fig. 5b the steady-state gain in the near forward direction decreases by a factor of 2 from that in Fig. 3 for $N_A = 10^{17}$ cm^{-3} while the gain in the backward direction drops by a factor of 5. This drop is because the gain in the backward direction is controlled by the maximum space charge field (E_q) that can be obtained at this short grating period ($\Lambda_g = .1\mu$m at $\lambda = .5\mu$m) and E_q is proportional to N_A, while the gain in the forward direction is mainly controlled by diffusion (E_D), which does not depend on the trap density.

Several other results can be inferred from Figs. 2 to 5. First, note that one might expect beam fanning (near forward scattering) to start over a wide range of angles and to coalesce to a smaller angular extent. This can be seen by comparing Figs. 2 and 3 for pump angles of $\theta_p = 10°$ to 40° and scattered beam angles θ_s equal to θ_p to $\theta_p + 90°$.

46

Second, since increasing the mobility by a factor of ten
from the baseline value used in Fig. 2 leads to dominance of
forward scattering over backscattering even at turn on, one
would expect that hole dominated crystals might be better
for producing backscattering. This is because one expects
hole mobilities to be smaller than electron mobilities.
This is generally what has been measured in $BaTiO_3$ (see the
review of mobility measurements in Ref. 27) and what is
found in semiconductors. Similarly, a comparison of Figs.
5a and 5b to Figs. 2 and 3 suggests that crystals with large
trap densities will favor backscattering over forward
scattering.

4. CONCLUSIONS

Plots of the gain-length product at turn on and in steady
state aid the understanding of many interesting features of
stimulated photorefractive scattering in $BaTiO_3$, such as the
occurrence of near forward and backscattering. These plots
can also be used as the coupling coefficient times length to
interpret four-wave mixing observations. The question that
these plots cannot answer is whether or not all of the rich
behavior seen in SPS in $BaTiO_3$[6] can be explained by time-
dependent, three dimensional calculations using these
coupling coefficients.

ACKNOWLEDGEMENTS

Table. Parameters of $BaTiO_3$,

Parameter, symbol	Value	Ref.
ordinary refractive index, n_o	2.505	28
extraordinary refractive index, n_e	2.434	28
electro-optic coefficient, r_{13}	24 pm/V	29
r_{33}	80 pm/V	29
r_{42}	1640 pm/V	30
dielectric constant, ϵ_{11}	3700	28
ϵ_{33}	150	28
total donor density, N_D	$2.-6.\ 10^{18} cm^{-3}$	31
trap density, N_A	$.2-1.\ 10^{17} cm^{-3}$	21
absorption coefficient, α	$0.6-3.5\ cm^{-1}$	31,32
mobility anisotropy, μ_{33}/μ_{11}	.1	25,26
mobility-lifetime product, $\mu\tau_R$	$10^{-10} cm^2/V$	26,27,33

REFERENCES

1. J.Feinberg, "Asymmetric self-defocusing of an optical beam from the photorefractive effect," J.Opt.Soc.Am. **72**, 46-51 (1982).

2. T.Y.Chang and R.W.Hellwarth, "Optical phase conjugation by backscattering in barium titanate," Opt.Lett. **10**, 408-410 (1985).

3. D.A.Temple and C.Warde, "Anisotropic scattering in photorefractive crystals," J.Opt.Soc.Am.B **3**, 337-341 (1986).

4. R.A.Rupp and F.W.Drees, "Light-induced scattering in photorefractive crystals," Appl. Phys. B **39**, 223-229 (1986).

5. J.Feinberg, "Self-pumped, continuous-wave phase conjugator using internal reflection," Opt.Lett. **7**, 486-488 (1982).

6. T.R.Moore, A.V.Novak, and R.A.Fisher, "Internal beam patterns in barium titanate phase conjugators: ring oscillators, half-rings, and translation-invariant patterns," Post-deadline paper PD12-1 presented at International Quantum Electronics Conference (IQEC '86), San Francisco, (1986).

7. N.Kukhtarev, "Kinetics of hologram recording and erasure in eletrooptic crystals," Pis'ma Zh. Tekh. Fiz. **2**, 1114-1116 (1976) [Sov.Tech.Phys.Lett. **2**, 438-440 (1976)].

8. G.C.Valley and M.B.Klein, "Optimal properties of photorefractive materials for optical data processing," Opt. Eng. **22**, 704-711 (1983).

9. I.R.Dorosh, Yu.S.Kuzminov, N.M.Polozkov, A.M.Prokhorov, V.V.Osiko, N.V.Trachenko, V.V.Voronov, and D.Kh.Nurligareev, "Barium-strontium niobate crystals for optical information recording," Phys.Stat.Sol. (a) **65**, 513-522 (1981).

10. V.V.Obukhovskii and A.V.Stoyanov, "Photoinduced light scattering in crystals with a nonlocal response," Kvantovaya Elektron. (Moscow) **12**, 563-570 (1985) [Sov.J.Quantum Electron. **15**, 367-371 (1985)].

11. G.Zhang, Q.X.Li, P.P.Ho, R.R.Alfano, S.Liu, and Z.Wu, "Dependence of specklon size on the laser beam size via the photoinduced light scattering in $LiNbO_3$:Fe," Appl. Opt. $\cancel{X}$, ^{25} XXX-XXX (1986).
2955-

12. E.M.Avakyan, K.G.Belabaev, and S.G.Odulov, "Polarization-anisotropic light-induced scattering in $LiNbO_3$:Fe crystals," Fiz. Tverd. Tela (Leningrad) **25**, 3274-3281 (1983) [Sov. Phys. Solid State **25**, 1887-1890 (1983)].

13. S.Odulov, K.Belabaev and I.Kiseleva, "Degenerate stimulated parametric scattering in $LiTaO_3$," Opt. Lett. **10**, 31-33 (1985).

14. G.Chanussot, V.M.Fridkin, G.Godefroy, and B.Jannot, "The photoinduced Rayleigh scattering in $BaTiO_3$ crystals showing the bulk photovoltaic effect," Appl. Phys. Lett. **31**, 3-4 (1977).

15. J.F.Lam, "Origin of phase conjugate waves in self-pumped photorefractive mirrors," Appl. Phys. Lett. **46**, 909-911 (1985).

16. A.Ashkin, G.D.Boyd, J.M.Dziedzic, R.G.Smith, A.A.Ballman, J.J.Levinstein, K.Nassau, "Optically-induced refractive index inhomogeneities in $LiNbO_3$ and $LiTaO_3$," Appl.Phys.Lett. **9**, 72-74 (1966).

17. R.Magnusson and T.K.Gaylord, "Laser scattering induced holograms in lithium niobate," Appl. Opt. **13**, 1545-1548 (1974).

18. W.Phillips, J.J.Amodei, and D.L.Staebler, "Optical and holographic storage properties of transition metal doped lithium niobate," RCA Rev. **33**, 94-109 (1972).

19. A.Litvinenko and S.Odoulov, "Copper-vapor laser with self-starting $LiNbO_3$ nonlinear mirror," Opt. Lett. **9**, 68-70 (1984).

20. N.V.Kukhtarev, V.Markov. and S.Odulov, "Transient energy transfer during hologram formation in $LiNbO_3$ in external electric field," Opt. Comm. **23**, 338-343 (1977).

21. M.B.Klein and G.C.Valley, "Beam coupling in $BaTiO_3$ at 442 nm," J.Appl.Phys. **57**, 4901-4905 (1985).

22. G.C.Valley, "Simultaneous electron/hole transport in photorefractive materials," J.Appl.Phys. **59**, 3363-3366 (1986).

23. F.P.Strohkendl, J.M.C.Jonathan, and R.W.Hellwarth, "Hole-electron competition in photorefractive gratings," Opt.Lett. **11**, 312-314 (1986).

24. K.R.MacDonald and J.Feinberg "Theory of a self-pumped phase conjugator with two coupled interaction regions," **73**, 548-553 (1983)

25. C.N.Berglund and W.S.Baer, "Electron transport in single-domain, ferroelectric barium titanate," Phys.Rev. **157**, 358-366 (1967).

26. C.-P.Tzou, T.Y.Chang, and R.W.Hellwarth, "Photorefractive measurement of anisotropy of the mobility of photo-excited holes in $BaTiO_3$," submitted to Proc.SPIE (1986).

27. M.B.Klein, "Physics of the photorefractive effect in $BaTiO_3$," Chap. 7 in **Photorefractive Materials and Applications**, eds. P. Günter and J.-P. Huignard, Springer, New York, (1986).

28. S.H.Wemple, $\ddot{}$ Didomenico,Jr. and I.Camlibel, Dielectric and optical properties of melt-grown $BaTiO_3$, J.Phys.Chem. Solids **29**, 1797-1803 (1968).

29. I.P.Kaminov, "Barium titanate light phase modulator," Appl. Phys. Lett. **7**, 123-125 (1965); erratum Appl. Phys. Lett. **8**, 54 (1966).

30. A.R.Johnston and J.M.Weingart, "Determination of the low-frequency linear electro-optic effect in tetragonal $BaTiO_3$," J.Opt.Soc.Am. **55**, 828-834 (1965).

31. M.B.Klein and R.N.Schwartz, "Photorefractive effect in $BaTiO_3$: microscopic origins," J.Opt.Soc.Am. B **3**, 293-305 (1986).

32. K.R.MacDonald, J.Feinberg, Z.Z. Ming, and P.Günter, "Asymmetric transmission through a photorefractive crystal of $BaTiO_3$," Opt. Comm., **50**, 146-150 (1984).

33. P.Günter, "Holography, coherent light amplification and optical phase conjugation with photorefractive materials," Phys. Repts. **93**, 199-299 (1982).

34. Y.Fainman, E.Klancnik, and S.H.Lee, "Optimal coherent image amplification by two-wave coupling in photorefractive $BaTiO_3$," Opt. Eng. **25**, 228 (1986).

35. B.Ya.Zel'dovich, V.I.Popovichev, V.V.Ragul'skii, and F.S.Faizullov, "Connection between the wave fronts of the reflected and exciting light in stimulated Mande'shtam-Brillouin scattering," ZhETF Pis. Red. **15**, 160-164 (1972) [trans. Sov. Phys. JETP Lett. **15**, 109-113 (1972)].

Figure Captions

Fig. 1 Geometry of the stimulated photorefractive scattering process in $BaTiO_3$.

Fig. 2 Gain length product per absorbed energy per unit volume, G_{to}, as a function of the angle between the scattered beam and the crystal c axis, θ_s, for pump angle to the c axis, θ_p, equal to 0 to 90° in steps of 10°. The trap density N_A equals 10^{17} cm^{-3} and the mobility lifetime product along the c axis is $\mu_{33}\tau_R = 10^{-10}$cm^2/Vs.

Fig. 3 Steady-state gain length product, G_{ss}, as a function of the angle between the scattered beam and the crystal c axis, θ_s, for pump angle to the c axis, θ_p, equal to 0 to 90° in steps of 10°. The trap density N_A equals 10^{17} cm^{-3}.

Fig. 4 Gain-length product per absorbed energy per unit volume as a function of the angle between the scattered beam and the c axis θ_s for pump angle to the c axis $\theta_p = 30°$, $N_A = 10^{17}$ cm^{-3} and $\mu_{33}\tau_R = 10^{-9}$cm^2/Vs.

Fig. 5 Gain-length products for a trap density of $N_A = 2 \times 10^{16}$ cm^{-3}, $\mu_{33}\tau = 10^{-10}$cm^2/Vs, and $\theta_p = 30°$. (a) Gain-length product per absorbed energy per unit volume as a

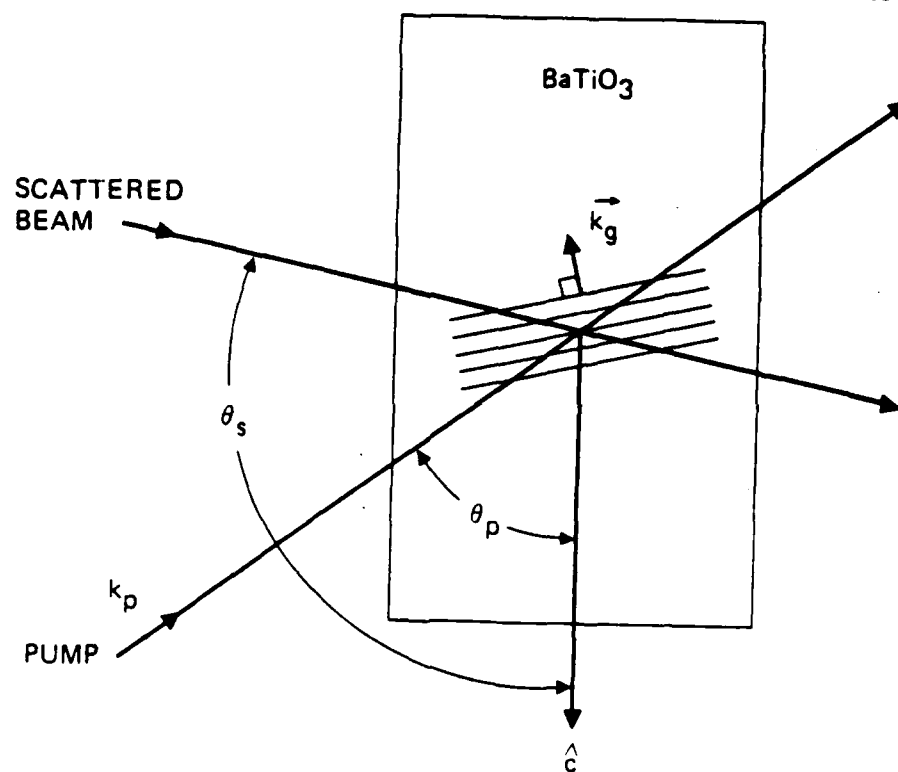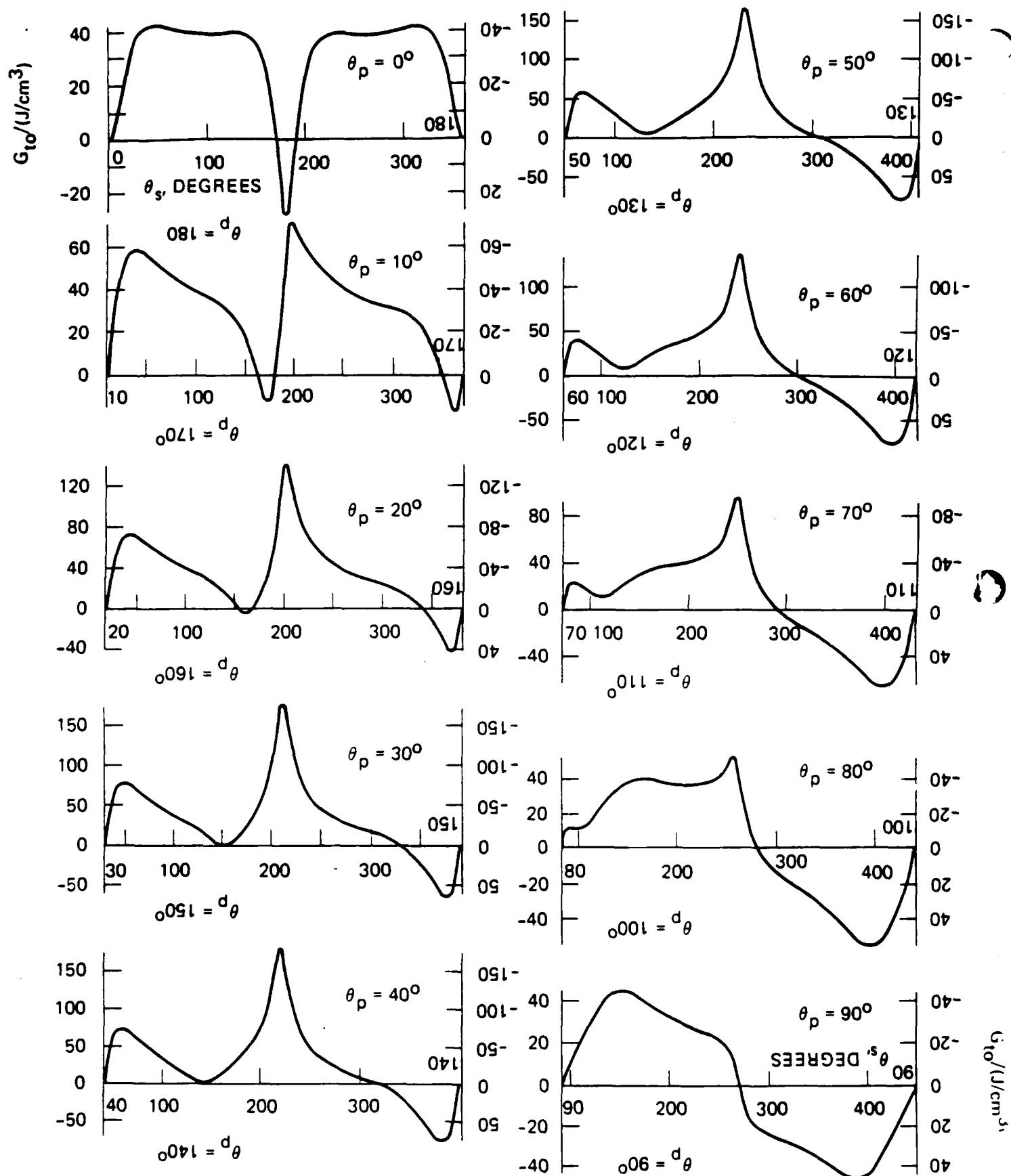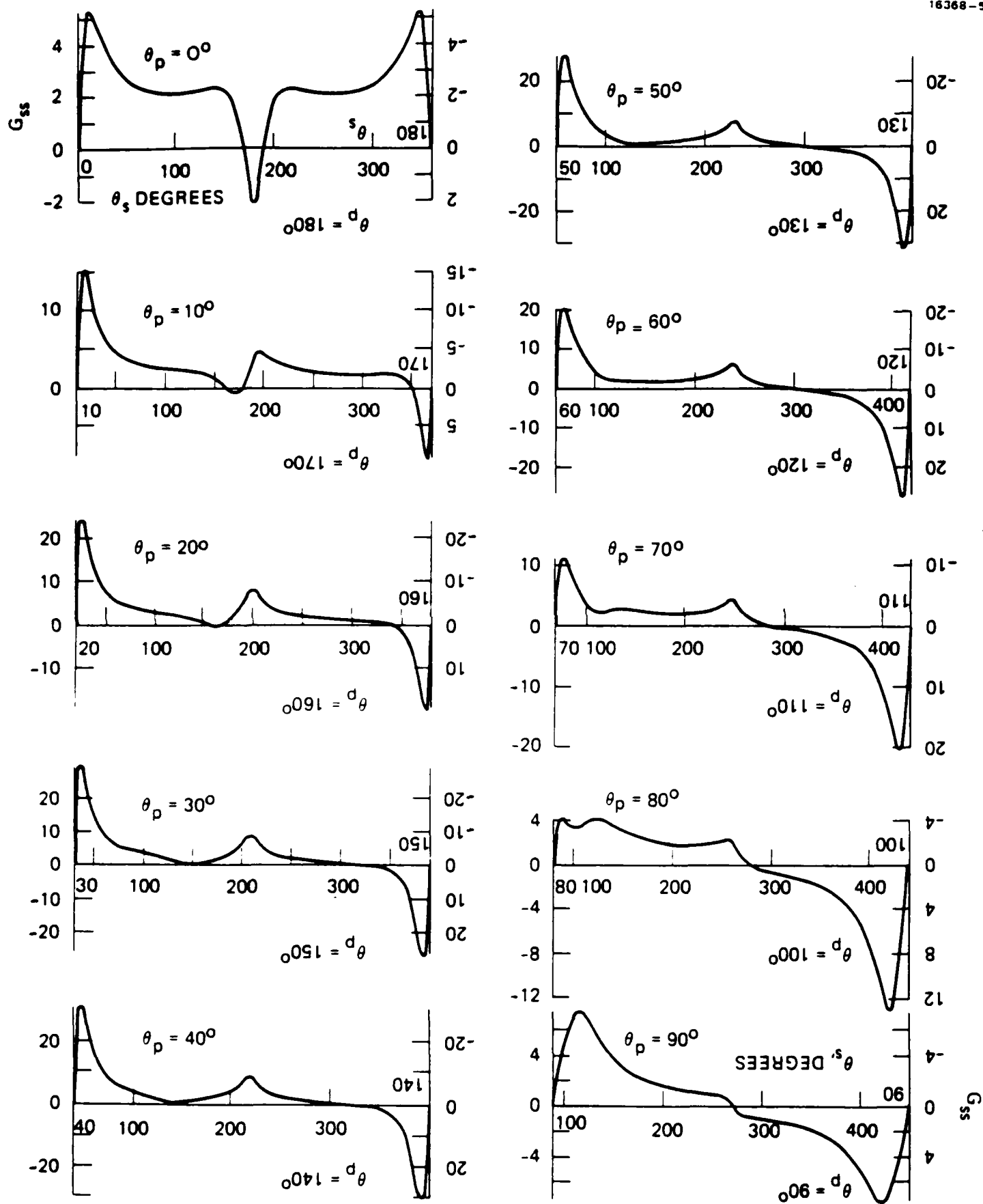function of θ_s. (b) Steady-state gain length product as a
function of θ_s.

Fig. 1

59

Fig. 2

60

Fig. 3

16368-5

Fig. 4
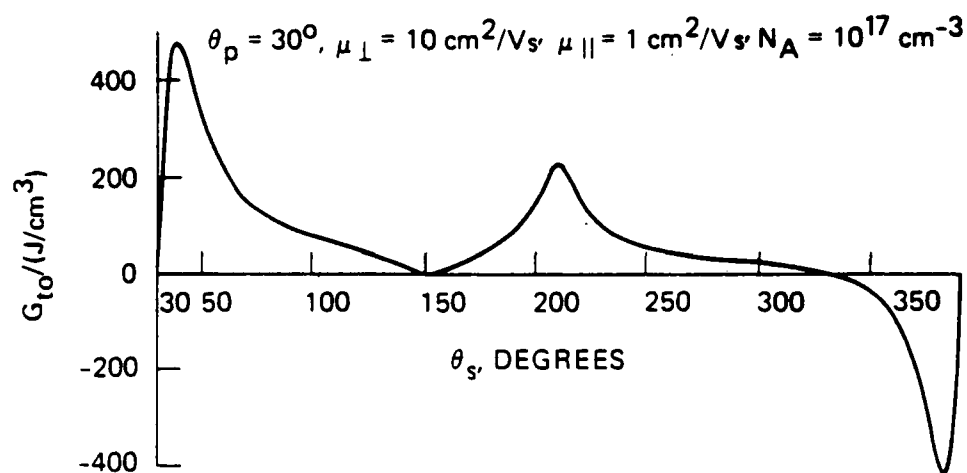
Fig. 5(a)

63

16368—2

$\theta_p = 30^\circ$, $N_A = 2 \cdot 10^{16}$ cm^{-3}
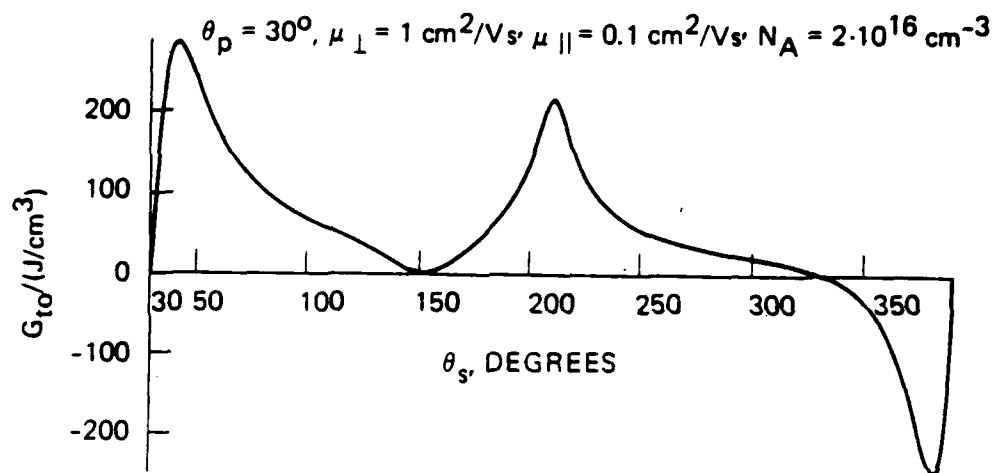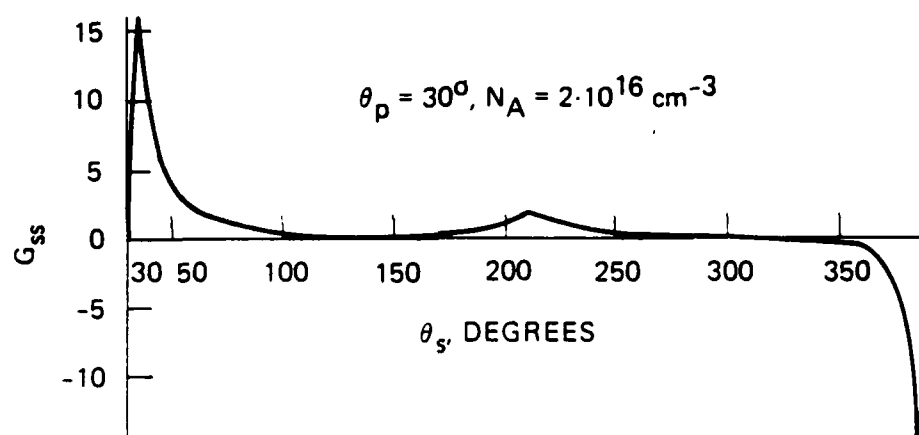
Fig. 5 (b)

APPENDIX 2

COMPARISON BETWEEN STIMULATED PHOTOREFRACTIVE SCATTERING AND STIMULATED RAMAN AND BRILLOUIN SCATTERING

In the propagation of light there is a close mathematical and conceptual analogy between photorefractive, Brillouin, Raman, and Rayleigh active media. As understanding of each field increases, the overlap appears greater and the differences appear to be more quantitative than qualitative. The underlying physics, which determines the coupling coefficients and time constants, is entirely different, but the coupled wave treatments are almost identical. Therefore, the contents of this chapter are germane to the study of stimulated Brillouin (SBS), Raman (SRS) and Rayleigh (SRLS) scattering. The term stimulated photorefractive scattering (SPS) can be used to emphasize the similarity. The field of phase conjugation has helped in the unification because photorefractive and Brillouin active media have emerged as the media of choice for many applications. This appendix gives a brief overview of SBS and SRS, and some references to the extensive literature.

In a Brillouin scattering event, an acoustic phonon is created in a medium when an incident (laser) photon is absorbed and a Stokes, or lower energy, photon is emitted. The density of the medium is coupled to the optical field through the electrostrictive force. In the stimulated process (SBS), two optical and one hypersonic wave are coherently coupled. The interference between two optical plane waves is a periodic intensity distribution, characterized by the difference wavevector and the difference frequency. If the frequency and wavevector lie on the acoustic phonon dispersion curve, then electrostrictive forces can generate a phonon. In turn, the periodic change in dielectric constant, which propagates in unison with the acoustic wave, can scatter one optical wave into the other. This moving grating imposes a Doppler frequency shift. In the classical treatment of SBS, the medium is taken to

be an elastic continuum, driven by the electrostrictive force and damped by viscosity and thermal conductivity.

In a vibrational Raman scattering event, a molecule makes a transition from a v=0 state to a v=1 state when an incident (laser) photon is absorbed, and a Stokes, or lower energy, photon is emitted. The nuclear motion and the optical field are coupled because the molecular polarizability is a function of the vibrational coordinate. In the stimulated process (SRS), the molecular excitation and the optical waves are coherently coupled. The molecular excitation is a quadrupole excitation rather than a change in vibrational level populations, and can be thought of as an optical phonon in contrast to the acoustic phonon of SBS. Two optical waves can generate an optical phonon if their difference frequency is close to the vibrational resonance. At the same time, the periodic change in polarizability will scatter each optical wave into the other, through the creation of sidebands separated by the vibrational frequency. In the classical treatment, the molecules are taken to be independent harmonic oscillators, damped by collisions and driven by a force derived from the dependence of the electrostatic stored energy density on the vibrational normal coordinate.

In backward SBS, the laser wave at ω_L and the Stokes wave at ω_S are counterpropagating. On resonance and in steady state, the coupling is described according to the following equations:[1]

$$\frac{dI_S}{dz} = -g_B I_L I_S + \alpha I_S, \qquad g_B = \frac{\omega_S^2 \rho_0 \tau_B}{c^3 nv} \left(\frac{\partial \epsilon}{\partial \rho}\right)_T^2$$

$$\frac{dI_L}{dz} = -g_B I_L I_S - \alpha I_L .$$

Here $I = cn|E|^2/8\pi$, ρ_o is the average density of the medium, τ_B is the lifetime of the acoustic phonon, v is the sound velocity, n is the index of refraction, ϵ is the dielectric constant, and T is the temperature. These equations are identical in form to the SPS case, except for the absence of the denominator $I_\theta = I_L + I_S$.

66

The analogous equations for SRS are[1]

$$\frac{dI_S}{dz} = -g_R I_S I_L + \alpha I_S \; , \qquad g_R = \frac{8\pi^2 \omega_S N}{n^2 c^2 m\Omega} \left(\frac{\partial \alpha}{\partial q}\right)^2 \frac{1}{1 + \beta}$$

$$\frac{dI_L}{dz} = -g_L I_S I_L - \alpha I_L \; , \qquad g_L = \frac{\omega_L}{\omega_S} g_R \; .$$

Here N is the molecular number density, m is the reduced mass of the vibration, Ω is the vibrational frequency, q is the vibrational normal coordinate, $\partial\alpha/\partial q$ is the differential polarizability, and β is the depolarization ratio. If photon fluxes were used instead of intensities, the two equations would have equal coupling constants.

The equations for other forms of stimulated scattering (e.g., Rayleigh and polariton) are also similar.[1] We have neglected them because they are less well known than Raman and Brillouin scattering; not because they are less similar. In fact, the magnitude of the frequency shift in Rayleigh scattering is closer to the SPS shift than to any other.

Stimulated photorefractive scattering has several unique properties and several characteristics in common with the more conventional mechanisms (SBS, SRS, and SRLS). It is insightful considering just the steady state small signal regime. For example, a signal wave can be amplified by any of the four mechanisms. The gain is due to a coupling of pump and signal amplitudes; not to the release of any energy stored in the medium. The magnitude and direction of energy flow between two optical waves is determined by the sine of a phase shift between their mutual interference pattern and the associated index variation. Phase transfer is proportional to the cosine of the phase shift. If only one wave is present initially, the existence of gain is crucial for the buildup of a second wave from noise.

67

In conventional stimulated scattering, a non-zero phase shift occurs because the index variation lags a moving interference pattern. The resulting energy flow favors the lower frequency wave; i.e., the Stokes wave experiences gain.[*] Waves that are degenerate in frequency have a stationary interference pattern and will not exchange energy in steady state because the phase shift goes to zero. The conventional mechanisms only support traveling waves, so the amplitude also goes to zero, and the waves will not exchange phase either.

The photorefractive effect is unique in that a large phase shift and amplitude exist in the degenerate case, owing to the mechanism of charge diffusion. The electro-optic effect can arise from a static distortion of the lattice by the space charge field, which corresponds to a zero frequency phonon. In the non-degenerate case, fringe motion imparts an additional component to the phase shift, which can change the direction and magnitude of the energy transfer.

In conventional stimulated scattering media, the decay time is so short that the induced excitations do not typically travel to a region of pump intensity different from that of their origin. Thus, the gain experienced by a signal wave at a given point in space is a function of the pump intensity at that point only. A local relationship also holds for the photorefractive case.[**] However, the gain is independent of the pump intensity in the small signal limit: mathematically, because of the normalizing denominators in the coupled wave equations; physically, because a redistribution of trapped charge is driven by spatial variations in intensity rather than by absolute intensity.

---

[*] An exception occurs when absorptive heating is responsible for the interaction.
[**] The "nonlocal response" referred to in the literature indicates a non-zero phase shift instead.

Under certain conditions, SBS and SRS backscattering give rise to the wavefront reversed replica of an incident wave. Wavefront reversal in SBS was discovered first[2] and has been studied more thoroughly. The incident and reflected waves are nearly degenerate in frequency, so the latter is close to a time reversed replica of the former. The wavefront reversing characteristics of SRS were also identified long after backscattering was first observed.[3] The large frequency shift imposed upon the backward wave limits the use of SRS in, for example, double-pass distortion-correction scenarios.

A serpentine path argument has been offered to explain why SRS backscattering generates a wavefront reversed replica of an incident pump wave.[4] Of all the optical noise components at the exit face heading back into the medium, those whose amplitude and phase variations mimic those of the pump will experience the highest gain. This results because such waves will retrace the path of the pump and therefore will favor the regions of high intensity (high gain), and avoid the regions of low intensity (low gain).

In the past, most experimental realizations and theoretical treatments of wavefront reversal by SBS consisted of only one incident wave, focused into either a bulk medium or a waveguide. In contrast, wavefront reversal by SPS has always been implemented with four-wave mixing (FWM), which involves two additional incident waves--the counterpropagating pump waves. As an illustration of the overlap between the two disciplines, phase conjugation via FWM in Brillouin active media is now being studied.[5,6] Similarly, photorefractive backscattering in the conventional SBS geometry has been recently observed.[7] No frequency shift was detected on the reflected wave, but the expected shift was very small--on the order of Hz. In the case of SBS, the backscattered wave originates in scattering of the pump wave from random density variations. The origin of SPS is not well understood, but is thought to be from optical inhomogeneities caused by random space charge fields or defects.

The backscattered Stokes wave in SRS is usually accompanied by a forward going Stokes wave and a forward going anti-Stokes (higher frequency) wave.[8] The photorefractive analog has been recently identified as the compr.ition between backscattering (wavefront reversal) and forward scattering (the fanning effect).[9]

Table 1 illustrates the similarities and differences between SRS, SBS, and SPS. The stated values (e.g., the intensities), are meant to be only representative. Where the numbers vary more than an order of magnitude on either side of a given value, a range of values is given, at the risk of appearing to be all-inclusive. The entries perhaps say as much about what specific materials and regimes people have chosen to study, as they say about the nature of the three phenomena.

	Stimulated Raman Scattering	Stimulated Brillouin Scattering	Stimulated Photorefractive Scattering	
Type of media	solid, liquid, gas		electro-optic insulators	a
	bulk and waveguide		bulk	b
Nonlinear gain	$g \sim 5 \times 10^{-3}$ cm MW^{-1} c	$g \sim 10^{-2}$ cm MW^{-1} c	$10^{-1} < \gamma < 10^{2}$ cm^{-1}	
Linear loss	negligible	d	$10^{-1} < \alpha < 10^{1}$ cm^{-1}	
Frequency shift	10^{13} Hz 10^{3} cm^{-1} c	10^{10} Hz 10^{0} cm^{-1} c	10^{0} Hz 10^{-10} cm^{-1}	e
Response time/ bandwidth	10^{-12} sec 5 cm^{-1} c	10^{-9} sec 5×10^{-3} cm^{-1} c	$10^{-2} - 10^{2}$ sec $10^{-10} - 10^{-14}$ cm^{-1}	f
Steady-state on-resonance grating phase shift	90°		90°	g
Type of source	Nd:YAG, ruby, excimer		argon ion, HeCd, dye, semiconductor diode	
Intensity	$10^{6} < I < 10^{9}$ W cm^{-2}		$10^{-1} < I < 10^{2}$ W cm^{-2}	f
Pulse length	$10^{-13} - 10^{-7}$ sec h	$10^{-9} - 10^{-7}$ sec h	cw	f
Intensity gain threshold for self-pumped phase conjugation	$10 < gIl < 30$ i		$0 < \Gamma l < 10$	i
Most common grating type	reflection		transmission	

71

a) Semiconductors have also been used recently.

b) SPS is a problem called "optical damage" in $LiNbO_3$, for example, but waveguides have not been used to study the effect.

c) These values have been taken from Table 1 of Ref. 1, with permission.

d) Exceptions are resonant Raman scattering and stimulated thermal Brillouin scattering.

e) This is not a property of the medium alone: it depends on the light intensity.

f) A few pulsed experiments have been done (see, e.g., Ref. 10). The intensities have been larger than the norm, and the response times are approximately inversely proportional to the intensities.

g) This can vary with an applied dc electric field or an internal bulk photovoltaic field.

h) A few cw experiments have been done using waveguides.

i) For a discussion of these values see Refs. 4 and 11. The SPS values apply to FWM rather than to simple backscattering.

REFERENCES

1. W. Kaiser, M. Maier: "Stimulated Rayleigh, Brillouin and Raman Spectroscopy," in Laser Handbook, ed. by F.T. Arecchi and E.O. Schulz-Dubois (North-Holland Publ. Co., Amsterdam, 1972) pp. 1077-1150.

2. B. Ya. Zel'dovich, V.I. Popovichev, V.V. Ragulsky, F.S. Faizullov: JETP Lett. 15, 109 (1972).

3. B. Ya. Zel'dovich, N.A. Mel'nikov, N.F. Pilipetsky, V.V. Ragulsky: JETP Lett. 25, 36 (1977).

4. B. Ya. Zel'dovich, N.F. Pilipetsky, V.V. Shkunov: Principles of Phase Conjugation, Vol. 42 in Springer Series in Optical Sciences, ed. by T. Tamir (Springer-Verlag, Berlin, 1985).

5. R.L. Abrams, C.R. Giuliano, J.F. Lam: Opt. Lett. 6, 131 (1981).

6. A.M. Scott: Opt. Commun. 45, 127 (1983).

7. T.Y. Chang, R.W. Hellwarth: Opt. Lett. 10, 408 (1985).

8. Yu. E. D'Yakov, S. Yu. Nikitin: Sov. J. QE 12, 796 (1982).

9. G.C. Valley: to be published JOSA B 3, xxx (1987).

10. L.K. Lam, T.Y. Chang, J. Feinberg, R.W. Hellwarth: Opt. Lett. 10, 475 (1981).

11. M. Cronin-Golomb, B. Fischer, J.O. White, A. Yariv: IEEE JQE 20, 12 (1984).

APPENDIX 3

COHERENT COMBINING OF PULSED DYE OSCILLATORS
USING NONLINEAR PHASE CONJUGATION*

J.O. White, G.C. Valley and R.A. McFarlane
Hughes Research Laboratories
3011 Malibu Canyon Road
Malibu, CA 90265

ABSTRACT

We have obtained coherent operation of two pulsed dye lasers
by coupling them with a common phase conjugate end mirror. The
phase conjugate mirror operates via the photorefractive effect in
a crystal of $BaTiO_3$, through a four-wave mixing process which
requires no external pump beams. Both laser gain cells employ
Rhodamine 6G dye pumped by a 10 Hz, frequency doubled Nd:YAG
laser. To start the system, the two gain cells are made to lase
independently by inserting an additional conventional mirror into
each cavity. One cavity incorporates a prism beam expander and a
retroreflecting diffraction grating, and lases with a narrow
0.04 nm linewidth. The other cavity employes three dispersing
prisms, and lases with a, broader, 0.4 nm linewidth. The beams
transmitted through each conventional mirror interact in the
$BaTiO_3$ crystal to create index gratings. Diffraction from these
phase gratings ultimately gives rise to wavefront reversed
replicas of each incident wave. When the auxiliary mirrors are
removed, the gratings remain in the crystal, the broadband laser
slowly becomes spectrally narrow, and its center frequency shifts
to match that of the narrowband laser. The spectrum of this
laser becomes broad again if the narrowband master laser is
turned off. Another indication of coupling is the observation
that turning off either of the lasers reduces the output power of
the other laser. We have also demonstrated phase locking by
interfering the two output beams to produce a stationary
interference fringe pattern.

END

L-87

DTIC